Structure and IR-spectrum calculations for small SF_6 clusters

T. A. Beu[a] and K. Takeuchi
The Institute of Physical and Chemical Research (RIKEN), Wako-shi, 351-01 Saitama, Japan

(Received 12 June 1995; accepted 18 July 1995)

A new second order perturbation approach for evaluating the splittings and shifts of the vibrational bands of homogeneous molecular clusters, consistently treating degenerate normal modes, is described. The Hamiltonian of the system comprises harmonic and anharmonic intramolecular vibration terms, and the intermolecular potential. The anharmonic intramolecular contributions and the intermolecular potential are treated as a perturbation. A new site-site intermolecular potential model for SF_6, featuring exchange, dispersion, electrostatic and induction terms, is presented. The new potential, with the parameters adjusted according to the observed monomer transition dipole moment and reproducing the experimental temperature dependence of the second virial coefficient, is used to determine SF_6 cluster structures up to the hexamer and, by means of the new line shift formalism, to calculate the corresponding IR-spectra in the region of the ν_3 vibrational mode (at 947.968 cm^{-1}). The contributions of the various potential terms to the frequency shifts are analyzed and the leading interaction mechanism is confirmed to be the electrostatic one (implicitly the resonant dipole-dipole coupling). The theoretical spectra are shown to fairly describe the experimental evidence when considering only exchange, dispersion and electrostatic interactions. With the available atomic polarizabilities, induction seems to lead to a systematic redshift of the entire spectrum for all cluster sizes. The structure of the cluster vibrations is investigated in terms of the individual monomer vibrations and is correlated with the found geometrical cluster configurations.

I. INTRODUCTION

Investigation of the structure and dynamics of molecular clusters by spectroscopic methods, especially through microwave and IR techniques, has achieved outstanding advances in the last few years. However, the profound understanding of the intermolecular interaction mechanisms could not have been possible without the assistance of complex theoretical approaches, developed in order to facilitate the analysis of the observed spectra.

Over the last two decades there has been quite a great experimental and theoretical interest in the SF_6 clusters,[1–7,29,30] and especially in the spectroscopy of the bands attributed to the ν_3 vibrational mode of the monomer ($\nu_3 = 947.968\ cm^{-1}$). Obviously, the particular interest in the ν_3 mode has been mainly a consequence of the similarities between SF_6 and the more challenging UF_6 system.

Since the threefold degenerate ν_3 vibrational mode of SF_6 is IR-active, it can be excited by CO_2 laser radiation in IR predissociation experiments.[1–6] Typically, in such experiments a beam of clusters containing IR-active molecules is formed in a supersonic nozzle and expanded into a vacuum chamber, where an intramolecular mode of vibration is excited by the IR-radiation. Energy relaxation may subsequently lead to predissociation of the clusters, causing a decrease in the beam signal. As a direct result of the mutual interaction of the molecules within the cluster, the spectral bands that have been found appear shifted (and sometimes also split) with respect to the corresponding gas phase absorption frequencies. The information gained from such experiments is even more interesting when combined with a cluster size selection method, allowing for a more detailed theoretical interpretation. In their measurements on SF_6 clusters, Huisken *et al.*[5] have used the size-selection technique introduced by Buck and Meyer,[8] which is based on the deflection of the molecular beam by scattering from a secondary noble gas beam.

Unfortunately, quite often the observed IR-predissociation spectra display broad, rather poorly structured peaks. To reduce the congestion of lines and the partial overlapping of the cluster spectra, Heijmen *et al.*[6] have performed two-laser experiments. In such ''pump and probe'' experiments, the fixed-frequency probe laser labels cluster levels for a certain cluster species, while the pump laser is scanned to identify IR-predissociation frequencies connected with the labeled cluster states.

The most successful theoretical model employed up to now to quantitatively describe the frequency shifts of the ν_3 vibrational mode in the SF_6 clusters, has been the dynamical dipole-dipole interaction model of Geraedts *et al.*[1] This model explains the $(-2\lambda):\lambda$ ratio of the shifts of the observed parallel and perpendicular bands of the SF_6 dimer by simply adjusting the quantity λ, resulting from the analytical diagonalization of the dipole-dipole interaction. By using the monomer transition dipole moment $\mu_{01} = 0.388$ D of Fox *et al.*,[9] the model predicts a realistic intermolecular separation, although it operates with structureless monomers.

In the elaborate approach of van Bladel *et al.*,[7] the analytical formalism has been developed specifically for treating dimer frequency shifts in the first order of perturbation theory, with the focus on the SF_6, SiF_4, and SiH_4 dimers. The model potential calculations for $(SF_6)_2$, based on atom-atom exchange, dispersion, electrostatic and induction terms,

[a]On leave from the University of Cluj-Napoca, Department of Theoretical Physics, 3400 Cluj-Napoca, Romania.

 0021-9606/95/103(15)/6394/20/$6.00

result in a realistic dimer structure, confirm the dominant character of the resonant dipole-dipole coupling, but underestimate the corresponding line shifts, and do not establish any correlations between the obtained theoretical spectra, the individual monomer normal modes, and the found dimer structure. The main reason for the underestimation of the frequency shifts lies, in our opinion, in the inappropriate effective charges assigned to the atoms, which reproduce the monomer transition dipole moment of Fox *et al.* rather than the more recent and accurate value due to Kim *et al.*[10] Furthermore, the potential model of van Bladel *et al.* has not been fitted to any macroscopic properties (such as virial coefficients or viscosities). These very deficiencies have been the stimulus for our attempt to establish an SF_6-SF_6 potential model that more accurately describes the experimental evidence.

Recently we have published a second order perturbation approach for evaluating the frequency shifts of homogeneous molecular clusters.[11] The formalism consistently treats the degeneracy of the cluster states emerging from the identity of the constituent monomers, however, degenerate vibrational modes of the monomers are not being taken into account. The underlying idea, extracted from early publications of Buckingham[12] concerning the frequency shifts in the IR or Raman spectra of chromophores under the influence of a solvent, is to treat the anharmonic contributions to the intramolecular force field and the intermolecular potential as a quantum mechanical perturbation of the molecular vibrations (described in the normal mode representation). The resulting first order formulas are equivalent to those of Buck *et al.*,[13] nevertheless, in the more complex second order, substantial differences arise by considering the complete basis set of the state space.

In Sec. II B we present the generalized formulation of our previously published approach, which now also takes into account the degeneracy of the monomer vibrational states, an essential aspect for correctly calculating the frequency shifts of the SF_6 clusters corresponding to the threefold degenerate ν_3 mode. The potential model we employ to determine the geometrical structures and line shifts of the SF_6 clusters, comprising exchange, dispersion, electrostatic and induction contributions, is described in Sec. II C.

Basic input data for the cluster structure and frequency shift calculations (the harmonic monomer frequencies, the displacement l-matrix, and the transformed cubic force constants ϕ_{rst}) are derived as part of the normal mode analysis of the monomer. The accurate treatment of the SF_6 monomer spectroscopy implies the refinement of the intramolecular force field and the result of this approach, as well as the transformation principles of the cubic force constants of SF_6 from valence to normal coordinates, are presented in Sec. III A.

The details of the adjustment procedure of the intermolecular potential parameters are described in Sec. III B. Although our potential model has a functional form similar to that of van Bladel *et al.*, the effective charges we have assigned to the atoms reproduce the more accurate monomer transition dipole moment value $\mu_{01}=0.437$ D of Kim *et al.*,[10] and the dispersion coefficients have been determined by fitting the calculated second virial coefficient to experimental data. In order to elucidate the role played by the induction coupling in the case of the SF_6 clusters, we employ two variants of our potential model: one neglecting the induction interactions, hereafter referred to as ''potential I,'' and the other one including them, hereafter called ''potential II.''

Section III C is devoted to the description of the structures we have obtained for the SF_6 clusters ranging from dimer to hexamer by using the two variants of the new potential model. The results, regarding binding energy, symmetry properties and geometrical size, are compared with those obtained by using other potential models from the literature, and the incremental binding energy of the clusters is examined.

In Sec. III D, the results of our frequency shift calculations, performed by means of the new perturbation formalism, are described in detail. The contributions to the frequency shifts from the various interaction mechanisms are analyzed and the theoretical spectra are compared with the experimental evidence and previous theoretical results. The appropriateness of the inclusion of the induction interactions in the potential model is also discussed. Finally, in Sec. III E the contributions of the individual monomer vibrational modes to the overall cluster vibrations are investigated, and the shifted spectral lines are correlated with vibrations of particular morphological monomer groupings within the clusters.

II. THEORETICAL MODEL

A. The Hamiltonian

The total cluster Hamiltonian may be written as

$$H=\frac{hc}{2}\sum_{r=1}^{3N-6}\sum_{m=1}^{M}\omega_r(p_{rm}^2+q_{rm}^2)+\frac{hc}{6}\sum_{r,s,t=1}^{3N-6}\sum_{m=1}^{M}\phi_{rst}q_{rm}q_{sm}q_{tm}+U, \tag{1}$$

where the first sum describes the uncoupled harmonic oscillations, the second sum is the anharmonic correction, while U represents the intermolecular potential. Here ω_r and ϕ_{rst} are the harmonic frequencies and the cubic force constants in units of wave numbers, respectively. q_{rm} and p_{rm} are position and momentum operators associated with the normal mode r of molecule m. M stands for the number of identical N-atomic molecules. The first two sums of the Hamiltonian (1) describe the conventional normal mode approach for the individual molecules including cubic anharmonicities.

The intermolecular potential U is a function of both the geometrical arrangement of the molecules within the cluster and the vibrational coordinates of each molecule. Taking into account the different orders of magnitude of the vibrational displacements of the atoms and the intermolecular separations, the interaction energy U may be cast in the form of a power series with respect to the normal coordinates

$$U=U_0+\sum_{r=1}^{3N-6}\sum_{m=1}^{M}\frac{\partial U}{\partial q_{rm}}q_{rm}+\frac{1}{2}\sum_{r,s=1}^{3N-6}\sum_{m,l=1}^{M}\frac{\partial^2 U}{\partial q_{rm}\partial q_{sl}}q_{rm}q_{sl}+\cdots, \tag{2}$$

where U_0 is the interaction energy of the molecules frozen in their equilibrium position and all derivatives are expressed with respect to this position keeping all but the explicitly implied normal coordinates constant.

In view of the fact that the Hamiltonian (1) is dominated by the harmonic term (first sum), which in addition allows for a full analytical diagonalization, providing a basis set for the Hilbert space of the cluster states, the anharmonic term and the intermolecular potential can be treated as a perturbation

$$W=\frac{hc}{6}\sum_{r,s,t=1}^{3N-6}\sum_{m=1}^{M}\phi_{rst}q_{rm}q_{sm}q_{tm}+U. \tag{3}$$

This approach is ultimately legitimated by the different orders of magnitude of the intra and intermolecular interaction forces, reflected by the generally higher intramolecular vibration frequencies (with typical values of 1000 cm^{-1}) than the intermolecular vibration frequencies (with typical values of 10–100 cm^{-1}).

B. Perturbation approach for cluster frequency shifts

In order to evaluate the fundamental frequency shift of a particular monomer normal mode due to the interaction of the molecules within the cluster, one has to determine the shifts of the ground state and of the first excited state of that specific normal mode. Within the framework of the stationary perturbation theory,[14] both the first and second order energy corrections are expressed in terms of the perturbation matrix elements, which, for further convenience, can be detailed in the present case as follows:

$$\begin{aligned}\langle\alpha_p^j|W|\alpha_n^i\rangle=&U_0\delta_{np}\delta_{ij}+\sum_{r=1}^{3N-6}\sum_{m=1}^{M}\frac{\partial U}{\partial q_{rm}}\langle\alpha_p^j|q_{rm}|\alpha_n^i\rangle+\frac{1}{2}\sum_{r=1}^{3N-6}\sum_{m=1}^{M}\frac{\partial^2 U}{\partial q_{rm}^2}\langle\alpha_p^j|q_{rm}^2|\alpha_n^i\rangle\\&+\frac{1}{2}\sum_{\substack{r,s=1\\r=s}}^{3N-6}\sum_{\substack{m,l=1\\m\neq l}}^{M}\frac{\partial^2 U}{\partial q_{rm}\partial q_{sl}}\langle\alpha_p^j|q_{rm}q_{sl}|\alpha_n^i\rangle+\frac{hc}{6}\sum_{r=1}^{3N-6}\sum_{m=1}^{M}\phi_{rrr}\langle\alpha_p^j|q_{rm}^3|\alpha_n^i\rangle\\&+\frac{hc}{2}\sum_{\substack{r,s=1\\r\neq s}}^{3N-6}\sum_{m=1}^{M}\phi_{rrs}\langle\alpha_p^j|q_{rm}^2q_{sm}|\alpha_n^i\rangle+\frac{hc}{6}\sum_{\substack{r,s,t=1\\r\neq s\neq t}}^{3N-6}\sum_{m=1}^{M}\phi_{rst}\langle\alpha_p^j|q_{rm}q_{sm}q_{tm}|\alpha_n^i\rangle.\end{aligned} \tag{4}$$

The eigenvectors of the unperturbed Hamiltonian may be set up as products of the state vectors for all harmonic normal modes of all molecules:

$$|\alpha_n^i\rangle=\prod_{r=1}^{3N-6}\prod_{m=1}^{M}|\alpha_{rm}^{ni}\rangle, \tag{5}$$

where, for each energy state n and degeneracy i, the set of integers $\{\alpha_{rm}^{ni}\}$ describes a particular combination of excitations of the individual normal modes of each molecule. Unfortunately, due to the fact that the degeneracy g_n differs for the different energy states, the notation $|\alpha_n^i\rangle$ is neither suggestive nor useful. Bearing in mind the typically low number of individual excitations that result in non-vanishing contributions to the matrix elements $\langle\alpha_p^j|W|\alpha_n^i\rangle$, a notation suggesting only the individual oscillator quantum states which differ from the ground state seems more eloquent. For example, the total cluster state in which the rth mode of the mth molecule is simply excited and the sth mode of the lth molecule is doubly excited could be represented by $|1_{rm}2_{sl}\rangle$.

As already pointed out, to determine fundamental line shifts, only the shifts of the ground state $|0\rangle$ and of simply excited states $|1_{ni}\rangle$ need to be evaluated, i.e. in expression (4) $|\alpha_n^i\rangle$ is either of form $|0\rangle$ or $|1_{ni}\rangle$. In view of the fact that the only non-vanishing matrix elements for q_{rm}, q_{rm}^2, and q_{rm}^3 imply states which differ by not more than three quanta, the only candidates for $|\alpha_p^j\rangle$ in formula (4) are of the form:

$$\begin{aligned}&|0\rangle,\\&|1_{rm}\rangle,\\&|2_{rm}\rangle,|1_{rm}1_{sl}\rangle,\\&|3_{rm}\rangle,|2_{rm}1_{sl}\rangle,|1_{rm}1_{sl}1_{tk}\rangle,\\&|4_{rm}\rangle,|3_{rm}1_{sl}\rangle,|2_{rm}1_{sl}1_{tk}\rangle,|1_{rm}1_{sl}1_{tk}1_{uj}\rangle.\end{aligned} \tag{6}$$

The relevant matrix elements of the powers of the individual normal coordinates q_{rm} are obtained by means of the standard harmonic oscillator algebra,[15] and are given in Appendix A.

In order to simplify notations by omitting the limits of the indices, the following convention will be used (except where otherwise specified): indices i through m stand for molecules, running over values from 1 to M, while indices n through t designate normal modes, running over values from 1 to $3N-6$.

The first order correction to the non-degenerate ground state energy is readily obtained as the mean value of the perturbation in the ground state

$$\epsilon_0^{(1)}=\langle 0|W|0\rangle=U_0+\frac{1}{4}\sum_r\sum_m\frac{\partial^2 U}{\partial q_{rm}^2}. \tag{7}$$

Since the present approach is conceived for clusters of identical polyatomic molecules with eventually degenerate vibrations, the degeneracy of a simply excited energy level E_n equals the product between the number M of molecules in the cluster and the degeneracy g_n of the implied monomer state, and under the influence of the intermolecular potential, the energy level is shifted and split up into g_nM sublevels E_{ni}. The corresponding first order energy corrections $\epsilon_{ni}^{(1)}$ result in eigenvalues of the perturbation matrix in the representation defined by the vectors $|1_{ni}\rangle$ which span the subspace Γ of the considered energy state. The perturbation matrix elements are given by

$$W_{ni,n'i'}\equiv\langle 1_{ni}|W|1_{n'i'}\rangle=\left(U_0+\frac{1}{4}\sum_r\sum_m\frac{\partial^2 U}{\partial q_{rm}^2}\right)\delta_{nn'}\delta_{ii'}+\frac{1}{2}\frac{\partial^2 U}{\partial q_{ni}\partial q_{n'i'}}.$$

Observing that the expression within parenthesis is that of the first order ground state correction, $\epsilon_0^{(1)}$, and defining the reduced perturbation matrix elements

$$\tilde{W}_{ni,n'i'}\equiv W_{ni,n'i'}-\epsilon_0^{(1)}\delta_{nn'}\delta_{ii'}=\frac{1}{2}\frac{\partial^2 U}{\partial q_{ni}\partial q_{n'i'}}, \tag{8}$$

the corresponding eigenvalue problem,

$$\sum_{n'\in\Gamma}\sum_{i'=1}^{M}[\tilde{W}_{ni,n'i'}-hc\Delta\nu_{ni}^{(1)}\delta_{nn'}\delta_{ii'}]c_{n'i',ni}=0,\qquad i=1,2,\ldots,M,n\in\Gamma, \tag{9}$$

directly yields the first order frequency shifts $\Delta\nu_{ni}^{(1)}=(\epsilon_{ni}^{(1)}-\epsilon_0^{(1)})/hc$ for the fundamental excitation from the ground state to the simply excited levels E_{ni}. As is apparent from definition (8) of the reduced perturbation matrix elements, the first order line shifts are independent of the intramolecular force constants, depending only on the curvature of the intermolecular potential. The diagonalization of the reduced perturbation matrix provides, besides the first order frequency shifts, the coefficients $c_{ni,n'i'}$ (as eigenvector components), which satisfy the completeness relation $\Sigma_{n'\in\Gamma}\Sigma_{i'}|c_{n'i',ni}|^2=1$, and which further enter the expressions of the second order line shifts.

The first order frequency shifts derived so far refer in principle to the harmonic monomer frequencies, which also characterize the unperturbed state of the cluster, i.e. the ideal state with harmonically vibrating independent monomers. In order to evaluate cluster line shifts with respect to observed monomer frequencies, only terms describing the influence of the intermolecular potential U have to be retained, eliminating terms depending *only* on the cubic intramolecular force constants, which merely account for the anharmonicity of the monomer frequencies. The first order line shifts, depending through the reduced perturbation matrix elements solely on the curvature of the intermolecular potential, hence refer both to the harmonic and observed frequencies, which turn out to be equally shifted to first order. Consequently, sticking to the convention to denote harmonic frequencies by ω, and anharmonic or observed frequencies by ν, the notation, $\Delta\nu_{ni}^{(1)}$, is justified.

The second order energy correction for non-degenerate states can be formally written in the case of the ground state:

$$\epsilon_0^{(2)}=-\sum_{p\neq 0}\sum_{j=1}^{g_p}\frac{|\langle\alpha_p^j|W|0\rangle|^2}{E_p^0},$$

being, as one may notice, essentially negative. Replacing in the above relation the non-vanishing perturbation matrix elements of the form $\langle\alpha_p^j|W|0\rangle$ given in Appendix A, one obtains after some term rearrangements:

$$\epsilon_0^{(2)}=-\frac{1}{2hc}\sum_r\sum_m\frac{1}{\omega_r}\left(\frac{\partial U}{\partial q_{rm}}+\frac{hc}{4}\sum_t\phi_{ttr}\right)^2-\frac{1}{8hc}\sum_{r,s}\sum_{m,l}\frac{1}{\omega_r+\omega_s}\left(\frac{\partial^2 U}{\partial q_{rm}\partial q_{sl}}\right)^2-\frac{Mhc}{48}\sum_{r,s,t}\frac{\phi_{rst}^2}{\omega_r+\omega_s+\omega_t}.$$

The terms depending only on the cubic force constants ϕ_{rst} (describing, as already pointed out, the anharmonic corrections of the monomer frequencies) have to be eliminated explicitly in the above relation. Thus, the expression of the second order ground state correction simplifies to

$$\epsilon_0^{(2)}=-\frac{1}{2hc}\sum_r\sum_m\frac{1}{\omega_r}\left(\frac{\partial U}{\partial q_{rm}}+\frac{hc}{4}\sum_t\phi_{ttr}\right)^2-\frac{1}{8hc}\sum_{r,s}\sum_{m,l}\frac{1}{\omega_r+\omega_s}\left(\frac{\partial^2 U}{\partial q_{rm}\partial q_{sl}}\right)^2. \tag{10}$$

In the case of simply excited states, $|1_{ni}\rangle$, the general second order energy correction for degenerate excited states takes the form[14]

$$\epsilon_{ni}^{(2)}=\sum_{n',n''\in\Gamma}\sum_{i',i''}c_{n'i',ni}c_{n''i'',ni}^{*}\epsilon_{n'i',n''i''}^{(2)},\qquad n\in\Gamma,i=1,2,\ldots,M,$$

with

$$\epsilon_{n'i',n''i''}^{(2)}=\sum_{p\notin\Gamma}\sum_{j=1}^{g_p}\frac{\langle 1_{n''i''}|W|\alpha_p^j\rangle\langle\alpha_p^j|W|1_{n'i'}\rangle}{E_n^0-E_p^0}.$$

Replacing the non-vanishing perturbation matrix elements of the form $\langle\alpha_p^j|W|1_{ni}\rangle$ listed in Appendix A, and employing in principle the same techniques as for the second order ground state correction, one obtains for $\epsilon_{n'i',n''i''}^{(2)}$ after some quite cumbersome calculations:

$$\epsilon^{(2)}_{n'i',n''i''}=-\frac{\delta_{n'n''}\delta_{i'i''}}{4}\sum_r\frac{3-\delta_{rn'}}{\omega_r}\left(\frac{\partial U}{\partial q_{ri'}}+\frac{hc}{4}\sum_t\phi_{ttr}\right)\phi_{n'n'r}-\frac{(1-\delta_{n'n''})\delta_{i'i''}}{8}\sum_r\frac{4+\delta_{rn'}+\delta_{rn''}}{\omega_r}$$
$$\times\left(\frac{\partial U}{\partial q_{ri'}}+\frac{hc}{4}\sum_t\phi_{ttr}\right)\phi_{n'n''r}+\frac{1}{4hc}\sum_{r\notin\Gamma}\sum_m\frac{1}{\omega_n-\omega_r}\frac{\partial^2U}{\partial q_{n'i'}\partial q_{rm}}\frac{\partial^2U}{\partial q_{n''i''}\partial q_{rm}}$$
$$-\frac{1}{4hc}\sum_r\sum_m\frac{1}{\omega_n+\omega_r}\frac{\partial^2U}{\partial q_{n'i'}\partial q_{rm}}\frac{\partial^2U}{\partial q_{n''i''}\partial q_{rm}}-\frac{\delta_{n'n''}\delta_{i'i''}}{2hc}\sum_r\sum_m\frac{1}{\omega_r}\left(\frac{\partial U}{\partial q_{rm}}+\frac{hc}{4}\sum_t\phi_{ttr}\right)^2$$
$$-\frac{\delta_{n'n''}\delta_{i'i''}}{8hc}\sum_{r,s}\sum_{m,l}\frac{1}{\omega_r+\omega_s}\left(\frac{\partial^2U}{\partial q_{rm}\partial q_{sl}}\right)^2. \tag{11}$$

Eliminating the terms depending only on the cubic force constants ϕ_{rst}, and observing that $\epsilon^{(2)}_0$ given by Eq. (10) cancels out the last two sums in the expression of $\epsilon^{(2)}_{n'i',n''i''}$, the second order line shift, $\Delta\nu^{(2)}_{ni}=(\epsilon^{(2)}_{ni}-\epsilon^{(2)}_0)/hc$, may be finally cast in the form

$$\Delta\nu^{(2)}_{ni}=\sum_{n',n''\in\Gamma}\sum_{i',i''}c_{n'i',ni}c^*_{n''i'',ni}\Delta\nu^{(2)}_{n'i',n''i''}, \tag{12}$$

where

$$\Delta\nu^{(2)}_{n'i',n''i''}=-\frac{\delta_{n'n''}\delta_{i'i''}}{4hc}\sum_r\frac{3-\delta_{rn'}}{\omega_r}\frac{\partial U}{\partial q_{ri'}}\phi_{n'n'r}-\frac{(1-\delta_{n'n''})\delta_{i'i''}}{8hc}\sum_r\frac{4+\delta_{rn'}+\delta_{rn''}}{\omega_r}\frac{\partial U}{\partial q_{ri'}}\phi_{n'n''r}$$
$$+\frac{1}{4(hc)^2}\sum_{r\notin\Gamma}\sum_m\frac{1}{\omega_n-\omega_r}\frac{\partial^2U}{\partial q_{n'i'}\partial q_{rm}}\frac{\partial^2U}{\partial q_{n''i''}\partial q_{rm}}-\frac{1}{4(hc)^2}\sum_r\sum_m\frac{1}{\omega_n+\omega_r}\frac{\partial^2U}{\partial q_{n'i'}\partial q_{rm}}\frac{\partial^2U}{\partial q_{n''i''}\partial q_{rm}}. \tag{13}$$

Generally, the most significant contributions to the second order line shifts are due to the first term of Eq. (13), coupling the generalized intermolecular forces $-\partial U/\partial q_{ri'}$ with the intramolecular force constants $\phi_{n'n'r}$. It is noteworthy that the second order shifts do not depend on *all* cubic force constants, but only on those implying states belonging to the subspace Γ of the considered normal mode. The last three sums in Eq. (13) are essentially less important due to the presence of the cubic force constants $\phi_{n'n''r}$ (coupling two different substrates $n',n''\in\Gamma$ with a third one) and of the second order derivatives of the intermolecular potential, respectively. However, through the resonance terms contained in the third sum, close lying levels can sometimes substantially contribute to the frequency shift.

The total frequency shift of a particular cluster spectral band obviously results from the sum of the corresponding first and second order shifts: $\Delta\nu_{ni}=\Delta\nu^{(1)}_{ni}+\Delta\nu^{(2)}_{ni}$.

An approach for the numerical evaluation of the intermolecular potential derivatives with respect to the internal coordinates, needed in the formulas of the frequency shifts, is described in Appendix B.

The relative importance of the cluster spectral lines corresponding to a particular vibrational mode can be judged on the basis of the transition strength, which can be calculated as the squared cluster transition dipole moment weighted by the degeneracy of the cluster state. In Appendix C we derive for the Cartesian components of the cluster transition dipole moment the approximate expression

$$\mu^\alpha_{01}=\frac{1}{\sqrt{2}}\sum_{n'\in\Gamma}\sum_m\left[\sum_a q_a\sum_{\alpha'}A^m_{\alpha\alpha'}\tilde{l}^{n'}_{a\alpha'}\right]c^*_{n'm,ni}, \tag{14}$$

where q_a are atomic charges, $A^m_{\alpha\alpha'}$ is the rotation matrix which characterizes the position of molecule m in the cluster, and $\tilde{l}^{n'}_{a\alpha'}$ are elements of the displacement l-matrix, which results from the normal mode analysis of the monomer.

C. The intermolecular potential model

One of the crucial aspects in performing structure and frequency shift calculations for clusters is the choice of a realistic intermolecular potential function. Due to the complexity of the calculations, it is desirable that the potential combines the ability of accurately describing various properties of the system with a relative analytical simplicity. From the potential energy hypersurfaces available in the literature, *site-site* potentials seem to be competitive candidates for tractable numerical solutions.

The functional form of the intermolecular potential we have chosen for calculating the structures of the SF_6 clusters and the corresponding vibrational frequencies shifts comprises exchange, dispersion, electrostatic, and induction terms. A similar model was previously employed by van Bladel *et al.*[7] for SF_6, SiF_4, and SiH_4 dimer calculations. One of the important features of this potential type, is that being based on site-site interactions, it depends on the relative atom positions, thus implicitly depending on the internal monomer vibrational coordinates.

The repulsive exchange and the attractive dispersion interactions are represented by standard (exp-6) terms:

$$U^{\text{exch}}=\sum_{m=1}^{M-1}\sum_{m'=m+1}^{M}\sum_{i\in m}\sum_{j\in m'}A_{ij}\exp(-B_{ij}r_{ij}), \tag{15}$$

and

$$U^{\text{disp}}=-\sum_{m=1}^{M-1}\sum_{m'=m+1}^{M}\sum_{i\in m}\sum_{j\in m'}\frac{C_{ij}}{r_{ij}^6}, \tag{16}$$

respectively, where r_{ij} is the distance between atom i belonging to monomer m and atom j belonging to monomer m'. The electrostatic term

$$U^{\text{elec}}=\sum_{m=1}^{M-1}\sum_{m'=m+1}^{M}\sum_{i\in m}\sum_{j\in m'}\frac{q_iq_j}{r_{ij}} \tag{17}$$

implies the fractional effective charges q_i placed on the atoms, such as to account for the vibrational transition dipole moment of the monomer. The induction potential contains three-body terms:

$$U^{\text{ind}}=-\frac{1}{2}\sum_{m=1}^{M}\sum_{\substack{m'=1\\m'\neq m}}^{M}\sum_{\substack{m''=1\\m''\neq m}}^{M}\sum_{i\in m}\sum_{j\in m'}\sum_{k\in m''}\frac{\alpha_iq_jq_k}{r_{ij}^2r_{ik}^2}(\hat{\mathbf{r}}_{ij}\cdot\hat{\mathbf{r}}_{ik}),$$

describing the interaction between the charge q_j from molecule m' and the dipole induced at site i of molecule m by the charge q_k from molecule m''. In a simplified writing, which takes advantage of the interchangeable roles of the ''inducing'' charge q_j and of the ''probing'' charge q_k, evidencing at the same time the total induction field, the induction potential may be conveniently described by fourfold rather than sixfold sums:

$$U^{\text{ind}}=-\frac{1}{2}\sum_{m=1}^{M}\sum_{i\in m}\alpha_i\left|\sum_{\substack{m'=1\\m'\neq m}}^{M}\sum_{j\in m'}\frac{q_j\hat{\mathbf{r}}_{ij}}{r_{ij}^2}\right|^2. \tag{18}$$

In our calculations, we employ two variants of the above potential model: the first one, designated in what follows as ''potential I,'' does not include the induction term, while the second, denoted as ''potential II,'' includes all the interactions.

III. RESULTS

A. Intramolecular force field of SF_6

As shown in Appendix B, for the evaluation of the intermolecular potential derivatives with respect to the vibrational coordinates ($\partial U/\partial q_{rm}$, $\partial^2U/\partial q_{rm}^2$, and $\partial^2U/\partial q_{rm}\partial q_{sl}$) occurring in the frequency shift expressions, the so-called l-matrix of the monomer is needed. The l-matrix describes the linear relationship between the Cartesian displacement and the normal coordinates of the atoms and results as part of the normal mode analysis of the monomer, performed according to the well-known G-F method of Wilson.[15] Within the present approach, the l-matrix (besides the cubic force constants ϕ_{rst}) thus models the coupling between the intra- and intermolecular force fields.

The molecules and ions of the type XY_6 have been proved to possess in most cases O_h symmetry. The SF_6 monomer conforms to this symmetry and, according to the irreductible representations of the O_h point group,[16] it follows (by applying the selection rules) that such a structure will give rise to one nondegenerate type A_{1g} vibration (ν_1), one doubly degenerate type E_g vibration (ν_2), two coupled triply degenerate type F_{1u} vibrations (ν_3, ν_4), one triply degenerate type F_{2g} vibration (ν_5), and one triply degenerate type F_{2u} vibration (ν_6). The F_{1u} vibrations are IR-active, while the A_{1g}, E_g, and F_{2g} vibrations are Raman active. The symmetry coordinates corresponding to the above symmetry species are described by Pistorius.[17]

TABLE I. Experimental vibrational frequencies ν_i [McDowell *et al.*(Ref. 19)] and refined quadratic symmetry force constants F_{ij} for the SF_6 monomer.

i	Γ_i	ν_i (cm^{-1})	F_{ij} (mdyn/Å)	
1	A_{1g}	773.6	6.69896	
2	E_g	642.1	4.61508	
3,4	F_{1u}	947.968	5.30319	
		615.03	−0.89981	1.03430
5	F_{2g}	522.9	0.76516	
6	F_{2u}	346.0	0.67003	

In our calculations on the SF_6 monomer, we have employed the S-F bond length of 1.564 Å found by Ewing *et al.*[18] in an electron diffraction study, and the quadratic intramolecular force field derived by McDowell *et al.*[19] from conventional IR-, diode laser-, and Raman spectra. Regarding the force field, the accuracy of the listed symmetry force constants F_{11}, F_{22}, F_{33}, F_{34}, F_{44}, F_{55}, and F_{66} is not sufficient to allow for the observed frequencies to be exactly reproduced. Moreover, since the second order frequency shifts of the ν_3 vibrational mode of SF_6, on which we focus in this work, typically amount to several tenths of a cm^{-1}, as will be shown in Sec. III D, implying the decimal digits of the resulting frequencies, a previous refinement of the force constants provided by McDowell *et al.* is necessary. The refinement procedure was accomplished using the ASYM20 program of Hedberg and Mills[20] and the resulting force constants are listed, along with the observed frequencies, in Table I.

In Table II we give the l-matrix elements yielded by the normal mode analysis of the SF_6 monomer, and corresponding to one of the substates of the threefold degenerate ν_3 mode (for the two other substates, the same non-zero elements occupy the y and z columns, respectively). They should be regarded as Cartesian displacements of the implied atoms for the unitary increment of the normal coordinate.

In order to accomplish the transformation of the force constants from symmetry to normal coordinates, obtaining

TABLE II. Displacement l-matrix for the ν_3 mode of the SF_6 monomer (dimensionless).

	l_x	l_y	l_z
S atom	−0.78799	0.0	0.0
axial F atoms	0.43164	0.0	0.0
equatorial F atoms	0.04011	0.0	0.0

the cubic force constants ϕ_{rst} which enter the expressions of the second order line shifts, we have applied the L-tensor method of Hoy and co-workers.[21] The internal valence (or symmetry) coordinates R_i can be expressed in terms of normal coordinates Q_r by a non-linear transformation

$$R_i=\sum_r L_i^r Q_r+\sum_{r,s} L_i^{rs} Q_r Q_s+\sum_{r,s,t} L_i^{rst} Q_r Q_s Q_t+\cdots,$$

where the elements of the L-tensor, L_i^r, L_i^{rs}, L_i^{rst},..., have to be interpreted as first, second, and third order derivatives of the internal coordinate R_i with respect to the normal coordinates. In particular, the formula for the transformation of the cubic force constants from symmetry to normal coordinates is:

$$\phi_{rst}=\sum_{i,j,k} F_{ijk} L_i^r L_j^s L_k^t+\sum_{i,j} F_{ij}(L_i^{rs} L_j^t+L_i^{rt} L_j^s+L_i^{st} L_j^r).$$

Since for the SF_6 monomer only quadratic symmetry force constants, F_{ij}, are available, the transformed cubic force constants ϕ_{rst} merely account for the nonlinearity of the transformation of the quadratic force field of the monomer from symmetry to normal coordinates.

B. Intermolecular potential adjustment

In Sec. II C we have presented the two intermolecular potential models we have used in our structure and line shift calculations for the SF_6 clusters: potential I, neglecting the induction interactions, and potential II, including them. In order to make our models as realistic as possible, we have adjusted their parameters in accordance with two macroscopic aspects: the monomer transition dipole moment and the temperature dependence of the second virial coefficient.

Our first concern in modeling the intermolecular potentials was to choose the effective atomic charges q_i in such a way as to exactly reproduce the observed transition strength of the ν_3 vibration in the SF_6 monomer.

Up to now, irrespective of the approach used to describe the structures and frequency shifts of the SF_6 clusters, all the published results[1–7] were based on the monomer transition dipole moment $\mu_{01}=0.388\pm0.02$ Debye reported by Fox *et al.*,[9] ignoring the more recent and accurate value of 0.437 ± 0.005 D of Kim and co-workers.[10] Historically, the preference for the value of Fox *et al.* has probably been due to the fair explanation of the dimer spectrum obtained with the dipole-dipole interaction model of Geraedts *et al.*[1,2] Since in this approach for the description of the cluster spectrum it is sufficient to fit a global parameter λ, in terms of which the line shifts can be expressed as -2λ and λ, and which formally depends on the transition strength μ_{01}^2, the accuracy of the actual transition dipole moment is evidently not critical. This conclusion holds, however, only for the particular model of Geraedts *et al.*

The same monomer transition dipole moment value has been used later on in the more sophisticated approach of van Bladel *et al.*,[7] based on a site-site potential similar to the one we are employing. Since this approach deals with a dimer built up from monomers showing a realistic structure, the possibility arises to treat the normal mode vibrations by displacements of the atoms, which can contribute through associated effective charges to the description of the observed transition dipole moment. The effective charges assigned to the atoms in order to reproduce the experimental monomer transition dipole moment (0.388 D) have been $-0.565e$ for the fluorine atoms and, correspondingly, $3.39e$ for the sulphur atom.

As a reference for determining the effective atomic charges of the SF_6 monomer for both our potential models, we have considered the transition dipole moment value $\mu_{01}=0.437$ D of Kim *et al.* The effective charges have been calculated accordingly from the expression of the monomer transition dipole moment derived in Appendix C,

$$\mu_{01}^{\alpha}=\frac{1}{\sqrt{2}}\sum_a q_a \tilde{l}_{a\alpha}^n,$$

by imposing the additional condition of monomer neutrality. In the above relation a is the atom index and α is the Cartesian coordinate index. The $\tilde{l}_{a\alpha}^n$ components result from the l-matrix elements given in Table II by applying Eq. (B2). Thus, we obtain for the effective charges of the fluorine and sulphur atoms the values $-0.637e$ and $3.822e$, respectively. Since they are intended to describe a monomer property, the same charges can be employed in both our potential models.

As regards the coefficients A_{ij}, B_{ij}, and C_{ij}, defining the exchange and dispersion potentials given by Eqs. (15) and (16), they can be constructed from the coefficients A_{ii}, B_{ii}, and C_{ii} of the individual atomic species by applying the standard combination rules, $A_{ij}=\sqrt{A_{ii}A_{jj}}$, $B_{ij}=(B_{ii}+B_{jj})/2$, and $C_{ij}=\sqrt{C_{ii}C_{jj}}$. For sulphur and fluorine, among other atomic species, such coefficients have been reported by Spackman,[22] and have been used by van Bladel *et al.* in their dimer structure and line shift calculations. For A_{ii} and B_{ii}, describing the short range repulsive atom-atom interactions, we have considered the same values, obtained by Spackman from fits to accurate calculations based on the Gordon-Kim electron gas model.[23] As for the dispersion coefficients C_{ii}, describing the long range interaction of two non-polar species, they have been derived from experimental and theoretical atomic dipole polarizabilities and C_6 constants and are claimed to be accurate to only 5–15%. Moreover, in an attempt to model the fluorine and sulphur atom interactions within the SF_6 clusters, the dispersion coefficients of both atomic species are most likely to change due to the additional polarization effects, and thus become the main candidates to be adjusted in a fit procedure against experimental virial coefficients.

The second virial coefficient is a valuable synthetic quantity for the characterization of intermolecular potentials and many successful empirical and semi-empirical potential models have been obtained by fitting to experimental data for this property. The pair potential for two molecules is in general a function of 12 coordinates, three position coordinates and three Euler angles for each molecule. It is always possible to choose a coordinate frame in which one of the molecules is placed (unrotated) at the origin and thus, the second virial coefficient may be expressed as a sixfold integral over

the relative position $\mathbf{r}\equiv(r,\theta,\varphi)$ and rotation $\mathbf{\Omega}\equiv(\Phi,\Theta,\Psi)$ of the second molecule:[24]

$$B(T)=-\frac{N_a}{16\pi^2}\int_0^\infty r^2dr\int_0^\pi \sin\theta d\theta\int_0^{2\pi}d\varphi\int_0^{2\pi}d\Phi$$
$$\times\int_0^\pi \sin\Theta d\Theta\int_0^{2\pi}d\Psi\{\exp[-U(\mathbf{r},\mathbf{\Omega})/k_BT]-1\}.$$

With a view to evaluating the second virial coefficient of SF_6, we have investigated two classes of numerical approaches for high-dimensional integration: Monte Carlo techniques and deterministic non-product methods. Whereas non-product methods have turned out to be more efficient, we have extensively used the variants due to Stroud[25] and Evans and Watts.[26] However, showing a higher degree of accuracy, we have employed the method of Stroud, briefly outlined in what follows, to produce all our final results.

Let $\Sigma_n^{(k)}\equiv(\sigma_1^{(k)},\sigma_2^{(k)},...,\sigma_n^{(k)})$ for $k=1,2,...,2n$ be integration points in the n-dimensional Euclidean space E^n, with components

$$\sigma_i^{(k)}=\begin{cases}\sqrt{2/3}\,\cos(ik\pi/n) & \text{for odd } i\\ \sqrt{2/3}\,\sin(ik\pi/n) & \text{for even } i\end{cases},$$

and $\sigma_n^{(k)}=(-1)^k/\sqrt{3}$ for odd n. According to the method of Stroud, an integral over the n-dimensional hypercube $S^n\equiv[-1,1]\times[-1,1]\times\cdots\times[-1,1]$ may be evaluated by the formula

$$\int_{S^n}f(x)dx\simeq\frac{2^n}{2n}\sum_{k=1}^{2n}f(\Sigma_n^{(k)}). \tag{19}$$

The second virial coefficient is best evaluated by expressing it as a sum of integrals over finite subregions of E^6, which can be scaled to S^6 such that Eq. (19) can be applied.

Taking advantage of the O_h symmetry of the SF_6 monomer, by halving each angular integration interval one can reduce the relevant space of relative orientations for two molecules, implying the positional (θ,φ)—and the Euler (Φ,Θ,Ψ) angles, by a factor of 32. For obtaining our final results for the second virial coefficient, we have used a uniform spatial mesh, with the radial coordinate restricted to the interval [2,34] (Å), outside of which the integrand has been negligible for the considered potential models. The radial spacing has been taken equal to 2 Å, and the angular spacings equal to $\pi/8$, resulting in 13107200 integration points, which have been proved to ensure the convergence of the virial coefficient values with five exact digits for all temperatures.

Since, as can be seen from Fig. 1, the temperature dependence of the second virial coefficient we have obtained by considering the potential of van Bladel *et al.* (represented with squares) underestimates by 50 to 100 cm^3/mol the observed values, it is obvious that this potential is not sufficiently attractive in its long-range components. Consequently, in order to reproduce the observed temperature dependence of the second virial coefficient, the SF_6-SF_6 potential has to be made more attractive by increasing the dispersion coefficients, C_{ij}, which, besides, are quite inaccurate, as shown above. Unfortunately, in an attempt to fit the theoretical virial coefficients to the experimental evidence, one is faced with the difficulty of having to adjust the coefficients C_{ii} for both sulphur and fluorine (the coefficient for the S-F interaction automatically results from the combination rule). Because no supplementary prescription is available, we have found it reasonable to vary both dispersion coefficients proportionally.

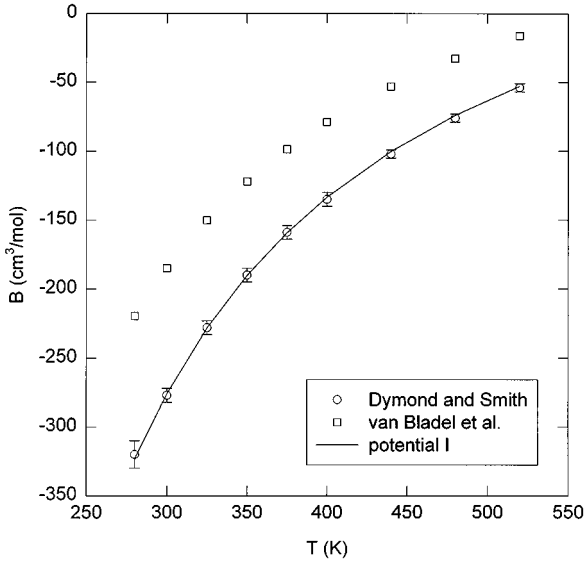

FIG. 1. Temperature dependence of the second virial coefficient of SF_6. With circles—the experimental values (Ref. 27); with squares—the values obtained using the potential of van Bladel *et al.* (Ref. 7); with continuous line—the dependence resulted using potential I.

In the case of potential I, we have achieved the best fit of the observed temperature dependence of the second virial coefficient by considering a 10.5% increase in the C_{ii} coefficients, yielding 8621.0 kJ/mol Å^6 for sulphur and 665.9 kJ/mol Å^6 for fluorine. For potential II, the increase of C_{ii} for an optimal fit amounts to 9.2%, resulting in 8519.6 kJ/mol Å^6 for sulphur and 658.0 kJ/mol Å^6 for fluorine. It is to be noted that the increase of the dispersion coefficients lies for both potential models within the error limit of 15% estimated by Spackman. The resulting root mean square deviations of 1.59 and 1.71 cm^3/mol, respectively, provide excellent fits in both cases. In Fig. 1, the temperature dependence of the virial coefficient resulting from potential I (plotted with continuous line) can be seen to nicely pass through the experimental error bars.[27] The corresponding curve for potential II cannot be practically distinguished.

For the polarizabilities α_i appearing in the induction term U^{ind} given by Eq. (18), we use the same values as van Bladel *et al.*

All relevant data for the description of our potential models, along with the parameters for the potential of van Bladel *et al.* are summarized in Table III.

In order to more clearly emphasize the decisive importance of the electrostatic terms in the description of the SF_6 cluster structures and line shifts, we have also investigated the Lennard-Jones type potential due to Powell *et al.*,[28]

TABLE III. Parameters for intermolecular potential models.

Potential model		A_{ii}(kJ/mol)	B_{ii}(Å^{-1})	C_{ii}(kJ/mol Å^6)	$q_i(e)$	$\alpha_i(a_0^3)$
Potential I	S	540857	3.132	8621.0	3.8250	
	F	336133	4.128	665.9	−0.6375	
Potential II	S	540857	3.132	8519.6	3.8250	7.2
	F	336133	4.128	658.0	−0.6375	5.1
van Bladel *et al.* (Ref. 7)	S	540857	3.132	7801.8	3.390	7.2
	F	336133	4.128	602.6	−0.656	5.1

$$U=-4\epsilon\sum_{m=1}^{M-1}\sum_{m'=m+1}^{M}\sum_{i\in m}\sum_{j\in m'}\left[\left(\frac{\sigma}{r_{ij}}\right)^6-\left(\frac{\sigma}{r_{ij}}\right)^{12}\right],$$

characterized by $\epsilon=0.14$ kcal/mol and $\sigma=2.8591$ Å . This potential implies interaction sites only at the fluorine atoms, not involving the sulphur atoms in any way. Lately it has been extensively used by Boutin *et al.*[29,30] in MD simulations concerning the structure and dynamics of $(SF_6)_M$ clusters in the size range $M=7-55$. Nevertheless, even though this potential has been accurately fitted to the experimental virial coefficients, not only does it not produce any relevant line shifts (not possessing any charges), but, as will be shown in Sec. III C, it results in an incorrect structure for the dimer.

In Figs. 2 and 3 we have plotted the atom-atom interaction potentials of Powell *et al.*, van Bladel *et al.*, and of this work for the fluorine and sulphur atoms. It should be clear that these potentials describe the atom-atom interactions within the SF_6 clusters, rather than those of the free atomic species, and can be regarded as projections of the SF_6-SF_6 potential energy hypersurface onto the respective atom-atom coordinates. In the case of our potential and of the potential of van Bladel *et al.*, we have not included the induction, which, as it will be later shown, is neither dominant for the cluster structures nor for the frequency shifts. As can be seen from Fig. 2, the F-F potential of Powell *et al.* is much more attractive than our potential and that of van Bladel *et al.* This behavior is partly caused by the fact that the F-F interactions have to account for all the interactions within the former model, including the very attractive S-F interactions. On the other hand, our potential and that of van Bladel *et al.* contain the repulsive contributions due to the charges assigned to the atoms with a view to reproducing the observed monomer transition dipole moment—our potential being slightly more attractive in the short-range region and more repulsive in the long-range region. Regarding the S-S and the S-F interactions depicted in Fig. 3, our curves lie outside those corresponding to the potential of van Bladel et al., that is, our S-S potential is more repulsive, while our S-F potential is more attractive.

C. Cluster structures

Cluster structure calculations can be straightforwardly performed by minimizing the total interaction energy of the cluster components. Taking into account the different nature of the interaction forces and the different orders of magnitude of the corresponding binding energies for the intra- and intermolecular degrees of freedom, a reasonable approach is to consider the molecules ''frozen'' in their equilibrium geometries and to minimize the intermolecular potential with respect to their relative positions. Moreover, such a technique is consistent with the overall philosophy of our ap-

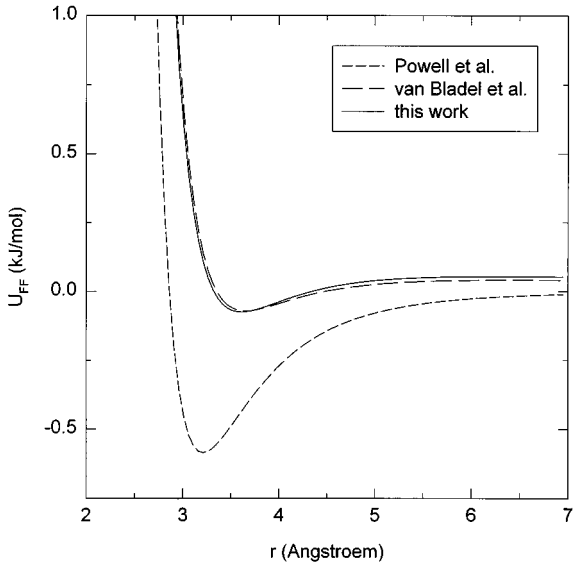

FIG. 2. Fluorine-fluorine interaction potentials within the SF_6 clusters (induction contributions are not included). With dotted lines—the potentials of Powell *et al.* (Ref. 28) and van Bladel *et al.* (Ref. 7).

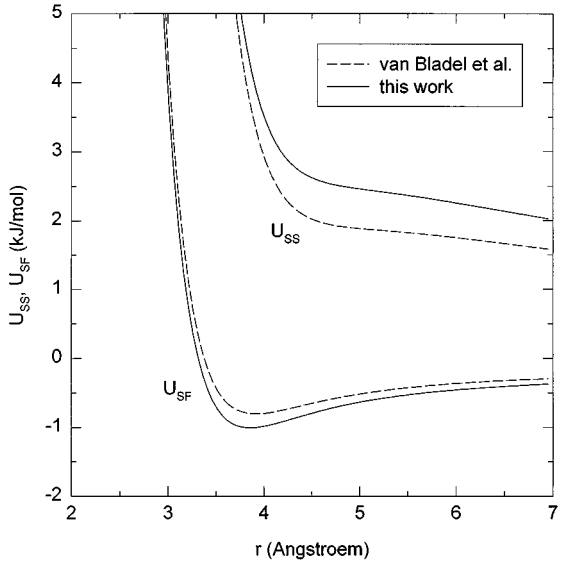

FIG. 3. Sulphur-sulphur and sulphur-fluorine interaction potentials within the SF_6 clusters (induction contributions are not included). With a dotted line—the potential of van Bladel *et al.* (Ref. 7).

TABLE IV. Calculated cluster structures by using the potential of van Bladel *et al.* (Ref. 7) potential I and potential II of this work. E represents the total binding energy (in kJ/mol), and d_{SS} is the average S-S distance (in Å). The second lowest dimer and tetramer (configurations $2'$ and $4'$) and the third lowest pentamer ($5''$) are included. The hexamer for the potential of van Bladel *et al.* does not show any symmetry.

	van Bladel *et al.*		Potential I		Potential II		
M	E	d_{SS}	E	d_{SS}	E	d_{SS}	Symmetry
2	−5.37	4.97	−6.68	4.90	−6.71	4.89	D_{2d}
$2'$	−5.02	5.08	−6.23	5.03	−6.33	5.01	C_{2h}
3	−14.96	5.07	−18.45	5.02	−18.79	5.00	D_{3d}
4	−27.27	5.24	−33.90	5.18	−34.49	5.16	D_2
$4'$	−27.11	5.23	−33.69	5.17	−34.30	5.16	C_3
5	−40.28	5.24	−49.93	5.18	−50.88	5.16	
$5''$	−39.93	5.22	−49.36	5.16	−50.12	5.15	C_{3h}
6	−54.63	5.21	−67.74	5.18	−68.69	5.16	C_{4h}

proach for frequency shifts. The positions and orientations of the molecules are specified by their center of mass Cartesian coordinates and Euler angles, which are optimized without constraints starting from randomly chosen initial configurations using the NAG library routine E04JAF. Typically, several hundreds (for the dimer) up to 5–6 thousands (for the hexamer) of minimizations are required to yield the global minimum, and a quite voluminous bookkeeping of the cluster configurations is necessary.

The results of our cluster structure calculations, by using the potential of van Bladel *et al.*, and the potentials I and II proposed in this work, are summarized in Table IV, where the binding energies and the mean S-S bond length of the clusters ranging from dimer to hexamer are listed. The mean S-S bond length is intended to give an idea about the ''compactness'' of the clusters. For all cluster sizes we have listed the data for the most stable (energetically lowest) isomer. However, since, as will be later emphasized, the second lowest dimer and tetramer configurations ($2'$ and $4'$) also show a remarkable symmetry, being energetically very close to the most stable isomers, we have considered them too. For the pentamer, the first symmetrical isomer is the third one ($5''$), and it is included as well. The geometrical configurations of all the listed cluster structures are presented in Figs. 4–8. It should be noted that the shape of the cluster structures is alike for all three discussed potential models with one exception: the hexamer resulted for the potential of van Bladel *et al.*, which, in addition, does not possess any symmetry.

We have depicted in Fig. 4 the two found dimers, the lowest having D_{2d} symmetry and the second, (reduced) C_{2h} symmetry. The C_{2h} symmetry structure offers a tempting explanation for the geared internal rotation of the dimer, in which it could play the role of intermediate configuration. Figure 5 shows the most stable trimer, exhibiting D_{3d} symmetry. Each monomer is connected to its neighbors by double S-F bonds, overlapping in the figure and providing a reminder of those of the second lowest dimer.

The two lowest tetramers, belonging to the D_2 and C_3 point groups, respectively, are represented in Fig. 6. The calculations of Geraedts *et al.*,[1] operating with structureless monomers, prescribe a T_d symmetry tetramer, which is the most compact structure resulting from four rigid spheres. It should be noted, however, that for both our tetramer configurations the positions of the sulphur atoms correspond to a slightly distorted T_d symmetry.

The most stable pentamer (Fig. 7) has no symmetry properties, being a distorted bi-pyramid. The first pentamer isomer with a well-defined (C_{3h}) symmetry (same figure), having a regular bi-pyramid shape, corresponds to only the third lowest configuration and a further manifestation of this peculiarity is its smaller average S-S distance as compared to the one for the most stable isomer.

The most stable hexamer, depicted in Fig. 8, again exhibits a nice C_{4h} symmetry for both of our potential models, unlike the hexamer resulting from the model of van Bladel *et al.*, which is unsymmetrical. Taking into account the quite close values of the in-plane distances between the S atoms contained in the ring and the out-of-plane S-S distances, it follows that the sulphur atoms are organized according to a slightly distorted O_h symmetry.

A general remark, which emerges from Table IV, is that for potentials I and II, the binding energies never differ by more than 1%, with the corresponding average S-S distances differing even less (at most by 0.4%). This indicates that the induction contributions, which differentiate our two models, are not determining for the cluster structures. As for the configurations obtained by using the potential of van Bladel *et al.*, their energies are typically more than 20% lower as compared to the ones obtained with our potentials. However, it is interesting to observe that the S-S distances again differ much less than the binding energies, being by only about 2% larger for the model of van Bladel *et al.* Thus, the geometrical size of the clusters shows little sensitivity to the electrostatic terms, evidencing the fact that SF_6 forms true van der Waals clusters, mainly bound by the dispersion attraction.

Irrespective of the potential model, dissimilar to the monotonous energy increase, there is a clear saturation tendency of the mean S-S distances with increasing cluster size, suggesting that for clusters larger than the tetramer, further accumulation of binding energy does not occur at the expense of enhanced ''compactness.''

In order to emphasize the tremendous differences which arise from different potential models, even if reproducing the temperature dependence of the experimental second virial coefficient, we show in Fig. 9 the only dimer structure which results from using the potential of Powell *et al.* It has D_{3d}

TABLE V. Contributions of the various potential terms to the dimer line shifts of the ν_3 mode (in cm^{-1}). Within parenthesis are given the first order results.

	Band	Exchange	Dispersion	Electrostatic	Induction	Total
Potential I	$\parallel$	0.20(0.28)	−0.12(−0.16)	−14.38(−14.72)		−14.32(−14.60)
	$\perp$	−0.12(−0.01)	0.07(0.02)	8.41(8.19)		8.36(8.20)
Potential II	$\parallel$	0.20(0.29)	−0.12(−0.16)	−14.45(−14.79)	−2.00(−2.01)	−16.30(−16.68)
	$\perp$	−0.13(−0.01)	0.07(0.02)	8.45(8.23)	−0.54(−0.55)	7.80(7.64)

symmetry (a threefold axis is in contradiction to the structure of the experimental spectra), its binding energy of −6.04 kJ/mol lies between the values obtained with our potentials and that of van Bladel *et al.*, whereas its average S-S distance is much lower (4.65 Å). This very compact structure is determined by the absence of the repulsive S-S interaction.

It is instructive to plot the incremental binding energy $E_M - E_{M-1}$ of the most stable isomers as a function of the cluster size M (Fig. 10). The pentamer does not conform to the general tendency of the curves, showing a reduced energy increment relative to the tetramer. This once more is a consequence of the reduced symmetry of the lowest pentamer. Although implying lower energy increments, the curve for the potential of van Bladel *et al.* has the same shape, evidencing the same specific behavior of the pentamer, whereas the curve obtained with the potential of Powell *et al.* suggests a very compact and stable pentamer, in spite of the fact that it possesses no symmetry at all.

D. Frequency shifts

In our band shift calculations for the SF_6 clusters, we have focused on the fundamental excitation of the ν_3 vibrational mode (at 947.968 cm^{-1}).

The most successful, and straightforward, of the theoretical models employed up to now to describe the frequency shifts of the ν_3 mode of the SF_6 dimer, has been the dynamical dipole-dipole interaction model of Geraedts *et al.*[1] The ν_3 absorption band is split up according to this model in a parallel band shifted by λ and a perpendicular band shifted by -2λ, the unit quantity $\lambda = (4\pi\epsilon_0)^{-1}\mu_{01}^2\langle R^{-3}\rangle$ resulting from the analytical diagonalization of the dipole-dipole coupling. Here, R corresponds to an averaged intermolecular separation and $\mu_{01} = 0.388$ D is the monomer transition dipole moment value reported by Fox *et al.*[9] In order to be consistent with their experimental data, Geraedts *et al.* have considered the unit value to be $\lambda = 6.8$ cm^{-1}, this choice also resulting in a reasonable value for the unknown intermolecular separation R. Unfortunately, being based on structureless monomers, and not yielding comparatively good results for the frequency shifts of the higher clusters, this model does not allow for interpretations correlated with realistic cluster structures.

On the other hand, the more elaborate first order perturbation approach of van Bladel *et al.*[7] yields a realistic dimer structure. The corresponding line shifts however underestimate the experimental findings, even though they are enhanced by adding induction contributions. In order to emphasize the crucial importance of the choice of the potential parameters, we will also discuss the line shifts we have obtained using the potential of van Bladel *et al.*, in spite of the increasing disagreements this model produces with increasing cluster size.

We have summarized in Table V the results of our frequency shift calculations for the most stable SF_6 dimer, both for potential I (including exchange, dispersion, and electrostatic terms) and potential II (additionally including induction contributions). As a result of the mutual interaction of the monomers within the dimer, the ν_3 vibrational mode is split up into a redshifted parallel band ($\parallel$) and a doubly degenerate blueshifted perpendicular band ($\perp$). In Sec. III E it

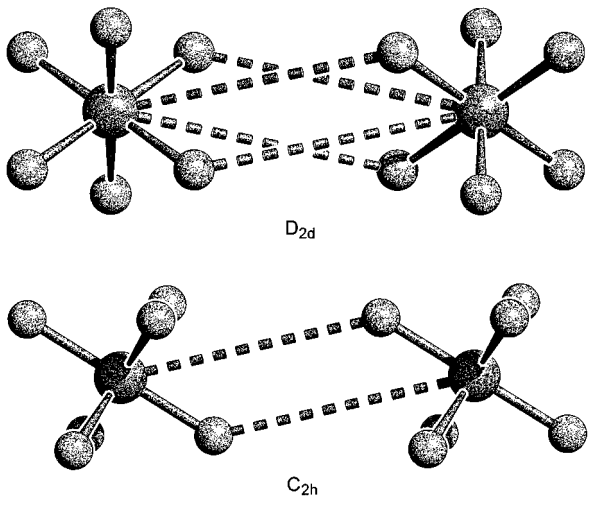

FIG. 4. Geometrical structures of the two dimer isomers found using potential I (D_{2d} is the lowest energy configuration). The shape of the corresponding isomers for potential II and the potential of van Bladel *et al.* (Ref. 7) is identical.

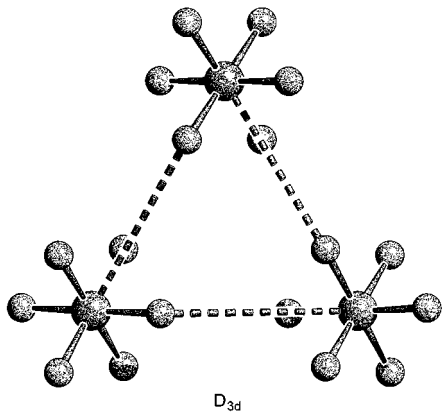

FIG. 5. Geometrical structure of the lowest trimer for potential I. Potential II and the potential of van Bladel *et al.* (Ref. 7) yield an identically shaped trimer.

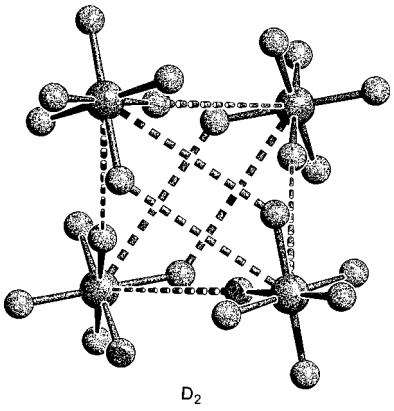

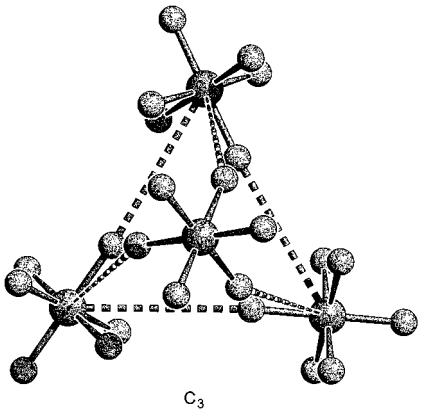

FIG. 6. Geometrical structure of the two lowest tetramers for potential I (D_2 is the lowest energy configuration). The shape resulted for potential II and the potential of van Bladel *et al.* (Ref. 7) is identical.

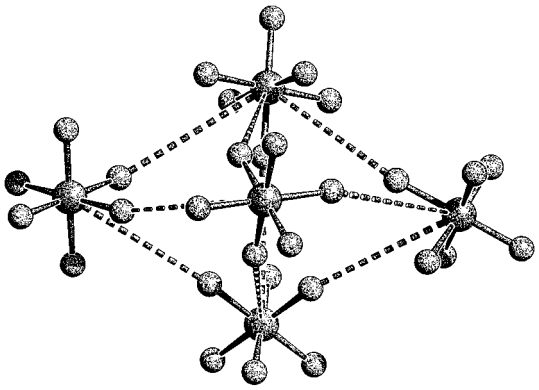

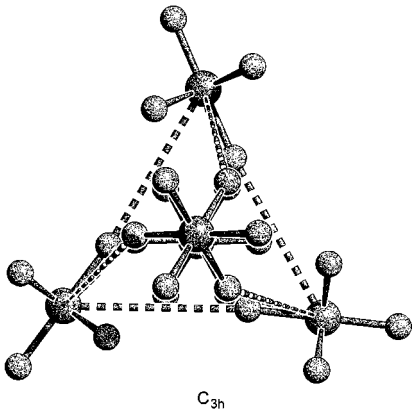

FIG. 7. Geometrical structure of the lowest and third lowest pentamers for potential I (the lowest energy configuration does not belong to any symmetry group). Potential II and the potential of van Bladel *et al.* (Ref. 7) yield identically shaped pentamers.

will be shown that the parallel band implies collective vibrations of the monomers along the longitudinal symmetry axis of the dimer, while for the perpendicular band, the resulting vibration takes place predominantly in a perpendicular plane. The differences between the line shifts corrected up to the second order and the first order results (added between parenthesis) represent the second order corrections, which typically amount to less than 0.4 cm^{-1}. The small second order corrections are a result of the relatively reduced anharmonicity of the normal monomer vibrations, but also of the small intermolecular potential curvature in the vicinity of the global minimum (the mixed second order derivatives $\partial^2 U/\partial q_{ni}\partial q_{rm}$ hardly exceed 0.7 cm^{-1}).

In order to identify the interaction mechanism which is mainly responsible for the frequency shifts, the individual contributions of the various potential terms to the line shifts have been evaluated by switching off the rest of the interactions, but considering the same dimer structure (obtained with the full potential model). It can be easily noticed that the electrostatic contributions are by far dominant, and by performing the molecular multipole analysis of the electrostatic interactions, taking into account the O_h symmetry of the monomer, it becomes clear that the vibrational dipole-dipole interaction, held responsible for the vibrational splittings in the literature,[1–7] indeed represents the leading mechanism. Furthermore, the effects of the exchange and dispersion couplings can be seen to be completely negligible. Whereas for the parallel band the exchange interaction produces a small blueshift and the dispersion an even smaller redshift (partially cancelling out the first one), in the case of the perpendicular band, the signs of the shifts are reversed. The induction, considered in potential II, contributes about 12% to the total frequency shifts, but as it will be further shown, its inclusion leads to a systematic redshift of the bands for all cluster sizes, turning out to be inappropriate with the available atomic polarizabilities. The implicit domi-

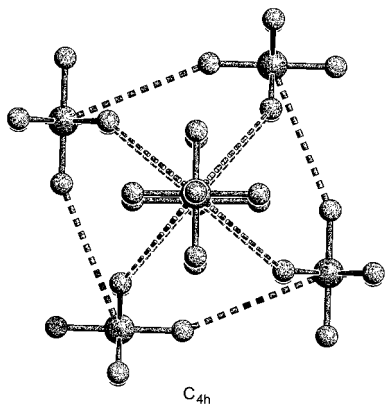

FIG. 8. Geometrical structure of the lowest hexamer for potential I. Potential II yields an identically shaped hexamer.

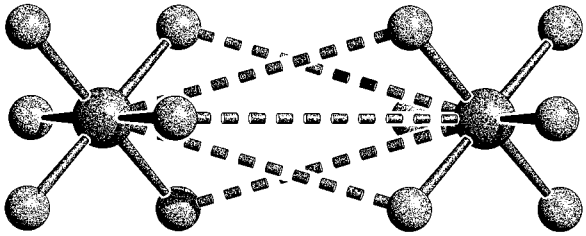

FIG. 9. Geometrical structure of the dimer found using the potential model of Powell *et al.* (Ref. 28).

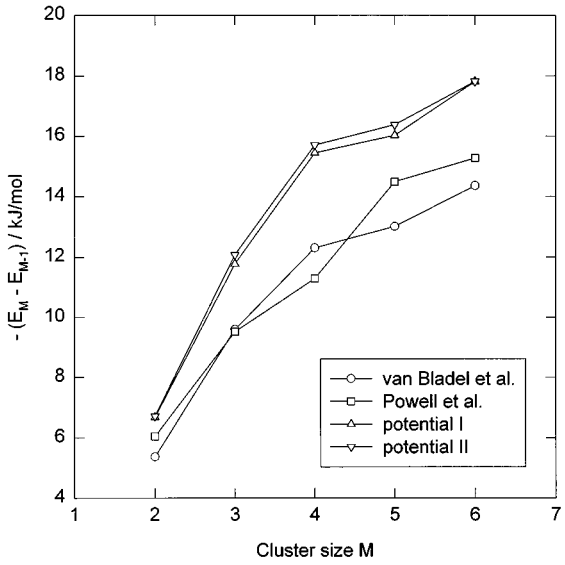

FIG. 10. Incremental binding energy of small SF_6 clusters. Open circles and open squares plot the values obtained using the potential of van Bladel *et al.* (Ref. 7) and that of Powell *et al.* (Ref. 28), respectively.

nance of the dipole-dipole resonance mechanism is, obviously, the ultimate explanation for the remarkable success of the simple model of Geraedts *et al.*

We have gathered in Table VI both experimental and theoretical data regarding the frequency shifts and line intensities for SF_6 clusters up to the hexamer. As experimental reference data we have chosen the results of the two most recently reported sets of measurements: the IR-IR double resonance experiments of Heijmen *et al.*,[6] and the vibrational predissociation experiments with size-selected clusters of Huisken *et al.*[5] The discrepancies between the estimated band positions are mainly due to the less sharper peaks in the predissociation spectra of Huisken *et al.* Nevertheless, the size-selectivity of the two-laser spectra of Heijmen *et al.* seems to be less effective. Unfortunately, no size-selected observed data for clusters higher than tetramer are available.

As a theoretical counterpart for our calculations, we have chosen the initial results of Geraedts *et al.*,[1] because the subsequently reported variants of their model did not bring any substantial improvements. For this model we have not included the hexamer, which, as a consequence of the fact that a compact symmetrical structure cannot result from spherical monomers, shows an unstructured spectrum of no interest for further comparison. We have not considered the results for the dimer obtained by van Bladel *et al.*[7] either,

TABLE VI. Experimental and computed line shifts $\Delta\nu_3$ (in cm^{-1}), and total transition strengths $g|\mu_{01}|^2$ (in D^2, within parenthesis) for SF_6 clusters up to the hexamer. For our calculations with the potential of van Bladel *et al.*, potential I and potential II, we give the results corrected up to the second order. In the case of the pentamer, we present the data for the third lowest isomer 5″, the first to show a well-defined symmetry. *g* represents the degeneracy of the spectral line.

M	Heijmen[a]	Huisken[b]	Geraedts[c]	van Bladel[d]	Potential I	Potential II	*g*
2	−14.1	−13.7	−13.6(0.30)	−12.3(0.30)	−14.3(0.38)	−16.3(0.38)	1
	8.4	7.7	6.8(0.60)	5.8(0.60)	8.4(0.76)	7.8(0.76)	2
3	−13.1	−13.0	−13.1(0.65)	−11.4(0.64)	−13.2(0.83)	−15.2(0.82)	2
	7.2	7.1	9.7(0.25)	7.4(0.26)	10.8(0.31)	9.8(0.32)	2
	15.3	15.3	13.6(0.45)	11.0(0.45)	16.3(0.57)	14.5(0.57)	1
4	−13.0	−12.9	−12.8(1.00)	−10.8(0.35)	−12.7(0.46)	−14.6(0.44)	1
	7.0	5.7	16.2(0.80)	−10.5(0.62)	−12.1(0.82)	−13.9(0.80)	2
	15.3	14.0		11.2(0.25)	17.1(0.30)	14.8(0.32)	1
				11.2(0.56)	17.1(0.69)	14.9(0.71)	2
5″			−13.9(0.40)	−10.8(0.37)	−12.3(0.50)	−14.3(0.48)	2
			−13.4(0.67)	−10.6(0.66)	−12.3(0.90)	−14.1(0.84)	1
			−5.8(0.30)	−6.6(0.30)	−7.6(0.40)	−8.8(0.39)	2
			17.9(0.80)	12.7(0.82)	19.8(1.00)	16.8(1.05)	2
			23.9(0.07)	14.0(0.09)	22.5(0.10)	18.4(0.11)	1
6					−12.3(0.24)	−14.8(0.24)	2
					−8.0(0.68)	−9.4(0.66)	1
					−7.6(1.44)	−8.9(1.38)	2
					17.8(0.46)	15.1(048)	1
					22.6(0.60)	18.5(0.67)	2

[a]Heijmen *et al.* (Ref. 6).
[b]Huisken *et al.* (Ref. 5).
[c]Geraedts *et al.* (Ref. 1); the tetramer lines are triply degenerate.
[d]Computed with the potential of van Bladel *et al.* (Ref. 7).

since we have included the results of our calculations using this potential. It should be stressed, however, that our first order line shifts for this potential coincide up to the first decimal digit with those reported by van Bladel *et al.*

For the pentamer we have considered only the third lowest isomer ($5''$), the first one to show a well-defined symmetry and consequently a structured spectrum which may be subject to intuitive interpretations. The total splitting of the ν_3 band of the most stable pentamer is for all potential models sensitively larger and the spectrum consists of more nonvanishing lines.

Already when comparing the theoretical line shifts for the dimer with the frequency shifts of -14.1 and 8.4 cm^{-1} evidenced by the IR-IR double resonance experiments of Heijmen *et al.*, it becomes apparent that the best agreement is achieved by using potential I (which does not include induction). It can be seen that the potential of van Bladel *et al.* underestimates the total splitting by more than four wave numbers, and the reason for this is obviously the smaller (less accurate) monomer transition dipole moment of Fox *et al.*,[9] which has been used to determine the effective atomic charges. In order to clarify whether the underestimation of the splitting cannot also be attributed to the different dispersion coefficients C_{ij}, we have increased the C_{ij} coefficients in the potential of van Bladel *et al.* to the values corresponding to potential I, but the changes in the frequency shifts have been minor. The crucial importance of the effective charges assigned to the atoms thus becomes clear. On the other hand, the inclusion of the induction interaction in potential II yields a poorer agreement with the observed spectra, leading to an overall redshift. It is, however, interesting to notice the same (2:1) intensity ratio of the perpendicular and parallel bands for all theoretical models, indicating again the leading contribution of the dipole-dipole interaction.

The fair agreement between our results for the dimer and the experimental evidence can also be noticed from Fig. 11, where we have depicted along with the two-laser spectrum of Heijmen *et al.*, the stick spectra for the two dimer structures found by considering potential I. The observed spectrum nicely accommodates the lines corresponding to both dimer isomers, suggesting that the experimental setup cannot discriminate them and that they possibly coexist under the given experimental conditions. Even though the units for the experimental and calculated spectra differ, the ratios of the corresponding line strengths seem to support the coexistence hypothesis, and this would further sustain the interpretation of the van der Waals geared rotation proposed in Sec. III C, as part of which the second lowest dimer could play the role of intermediate structure.

More than from the listed frequency shifts, the agreement between our dimer spectrum and the measurements of Huisken *et al.* becomes evident by inspecting Fig. 12, where the calculated lines seem to point to the highest attenuation values rather than to the maxima of the Lorentzian fit of the experimental points, the ratio of the calculated line strengths reproducing quite well the corresponding attenuation ratio.

In Fig. 13 we have plotted besides the two-laser spectrum of Heijmen *et al.* for the trimer, the corresponding stick spectrum resulted by using potential I. Although the structure

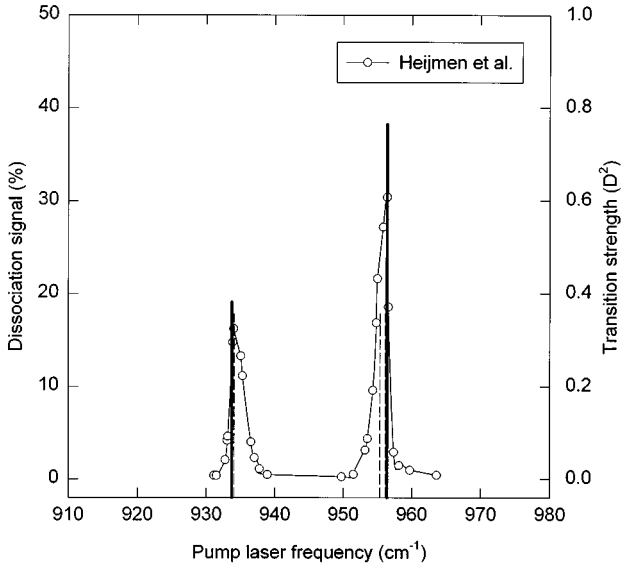

FIG. 11. Two-laser spectrum of the SF_6 dimer from Heijmen *et al.* (Ref. 6) and calculated stick spectrum using potential I. The thick lines correspond to the lowest isomer (D_{2d}) and the dotted lines to the second lowest one (C_{2h}).

of the spectrum and the position of the outer lines is well reproduced, the calculated middle line appears blueshifted by approximately 3.5 cm^{-1}. However, at about 955 cm^{-1}, where the experimental peak is located, important contributions from the dimer are likely to exist (see Fig. 11). As regards the results of Geraedts *et al.*, the underestimation of the total band splitting has become even more apparent than in the dimer case, as can be seen from Table VI. The same holds also for our calculations using the potential of van Bladel *et al.*, but to an even more critical extent. As for the results based on potential II, the lines are again redshifted too much.

Going to the tetramer (Fig. 14), a striking finding is the appearance of a supplementary peak at about 955 cm^{-1} in

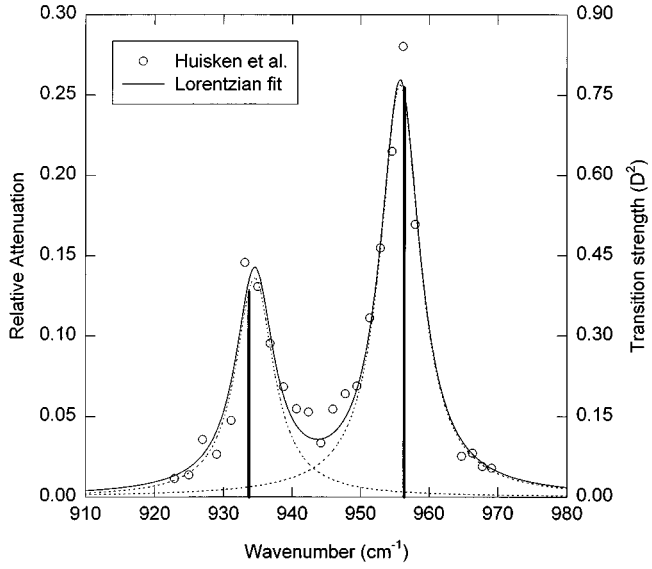

FIG. 12. Pure SF_6 dimer absorption and predissociation spectrum from Huisken *et al.* (Ref. 5) and calculated stick spectrum for the lowest isomer (D_{2d}) using potential I.

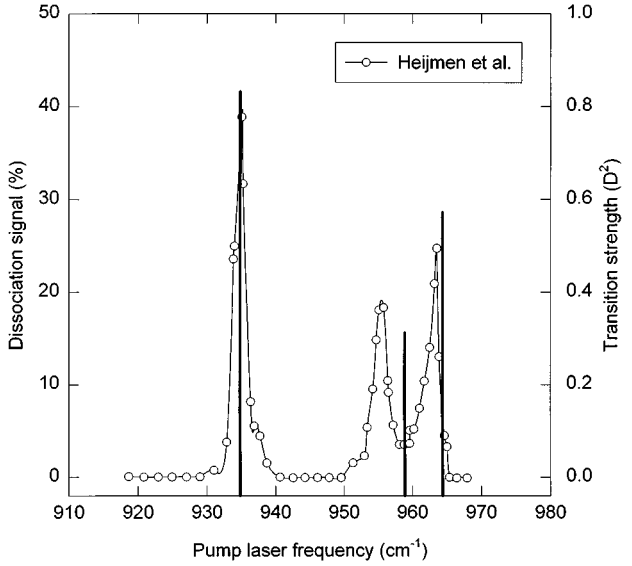

FIG. 13. Two-laser spectrum of the SF_6 trimer from Heijmen *et al.* (Ref. 6) and calculated stick spectrum using potential I.

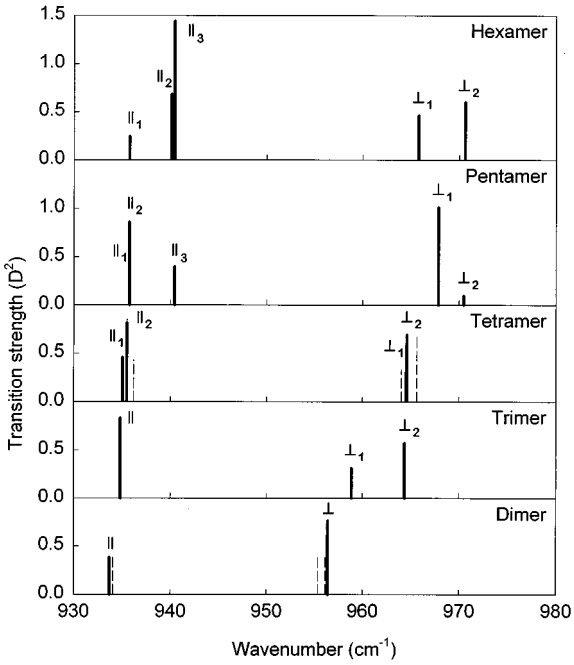

FIG. 15. Calculated stick spectra of SF_6 clusters from dimer to hexamer using potential I. The continuous lines correspond to the most stable isomers, while the dotted lines to the second lowest ones. For the pentamer, the third lowest configuration is being considered.

the IR-IR double resonance spectrum of Heijmen *et al.* with no theoretical counterpart. Nevertheless, judging from the fact that the results of Geraedts *et al.* predict two well separated bands as well, we tend to believe that the additional peak is to be assigned rather to the dimer or the trimer. There exists however a qualitative difference between the result of Geraedts *et al.* and the one we obtain: while the former predicts only two triply degenerate lines for the employed T_d symmetry tetramer, we find for all potential models two groups of two almost overlapping lines, in each group one being non-degenerate and the other doubly degenerate. The supplementary splitting of our tetramer lines is clearly a consequence of the slightly distorted T_d structure of both our tetramer configurations. Except for the above mentioned aspect, the agreement of our tetramer spectrum with the one of Heijmen *et al.* is satisfactory, the difference of about 1.8 cm^{-1} in the blueshifted band probably being due to the varying laser effectiveness in the marginal frequency region. Again, as in the case of the dimer, judging by the experimental bandwidths, the two tetramer isomers are not likely to be distinguished under the given experimental conditions. As for the tetramer spectrum of Huisken *et al.* (Fig. 6 of Ref. 5), due to the very low laser fluence (5.5 mJ/cm^2), the bands are quite diffuse, not allowing for a reliable quantitative comparison.

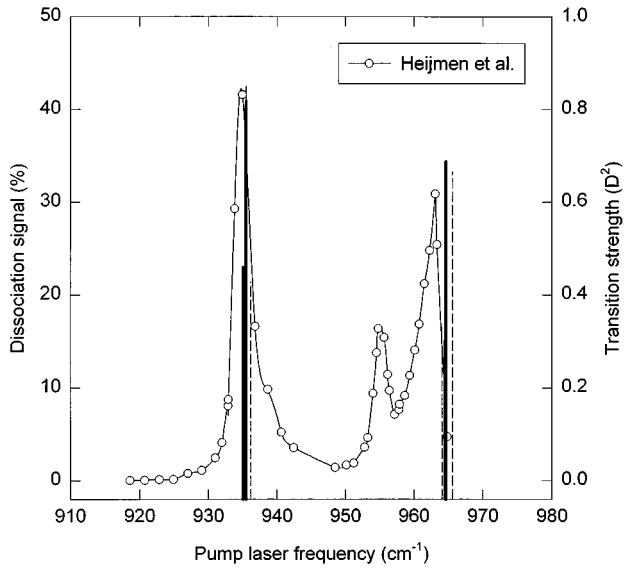

FIG. 14. Two-laser spectrum of the SF_6 tetramer from Heijmen *et al.* (Ref. 6) and calculated spectrum using potential I. The thick lines correspond to the lowest isomer (D_2) and the dotted lines to the second lowest one (C_3).

In a rather surprising manner, the agreement of the results of Geraedts *et al.* with the experiments improves for the tetramer over the trimer, while the potential of van Bladel *et al.* provides a too small total splitting in the spirit of the already noticed underestimating tendency. As regards our results for potential II, the overall redshifting tendency is somewhat diminished, suggesting that with increasing cluster size, the induction contributions become more and more important. The persistent discrepancies with respect to the experimental band shifts indicate, however, that more accurate polarizabilities are required for a subtle description of the cluster vibrations.

Figure 15 shows the stick spectra of the SF_6 clusters up to the hexamer, obtained by using potential I. The lines have been denoted according to the sign of the frequency shift: with $\parallel$ for redshifted lines and with $\perp$ for the blueshifted ones (the parallel or perpendicular character will be clarified in the next section). While the ''parallel'' lines tend to preserve the red boundary of the spectra at about 935 cm^{-1} with increasing cluster size, the ''perpendicular'' lines gradually

move toward higher frequencies, however with a saturation tendency, which brings about an almost non-varying total splitting when going from the pentamer to the hexamer. The same tendency can be also observed in Table VI in the case of potential II and this finding can be correlated with the saturation of the average S-S distance, which was discussed in Sec. III C. Apart from the supplementary splitting in the case of the tetramer, pentamer and hexamer, which is obviously due to the presence of monomers in non-equivalent positions, the parallel lines seem to be less sensitive to the ''compactness'' of the cluster (given by the average S-S distance) than the perpendicular lines.

E. Structure of the cluster vibrations

In this section we try to shed some light on the structure of the collective monomer vibrations, establishing correlations between the cluster configurations and the corresponding spectra. For the sake of conciseness we will confine the discussion to clusters up to the tetramer.

The ν_3 vibrational mode of the SF_6 monomer being threefold degenerate, in principle all three vibrations along the local Cartesian coordinates will take part in the overall vibration of the cluster. We will graphically symbolize each component of the vibration by a vector along the respective local Cartesian axis, implying individual vibrations of the atoms with relative amplitudes given by the l-matrix components listed in Table II (with all fluorine atoms moving in phase in the direction of the vector, and the sulphur atom moving out of phase in the opposite direction). The amplitudes of the defined vibration vectors will be given by the coefficients $c_{n'i',ni}$, representing the weights of the individual vibrational states within the total cluster state, $|\Psi_n^i\rangle = \Sigma_{n' \in \Gamma} \Sigma_{i'} c_{n'i',ni} |1_{n'i'}\rangle$, and resulting as eigenvector components from the eigenvalue problem (9) for the reduced perturbation matrix.

In Fig. 16 we have depicted the parallel ($\|$) and perpendicular ($\perp$) vibrations for the most stable dimer configuration, along with the parallel vibration for the second lowest isomer. In the case of the parallel vibrations, the fluorine atoms vibrate solidary in phase along the dimer axis, like a cage, while the two sulphur atoms vibrate out of phase along the same axis (the vibration components for the second lowest isomer are symmetrical with respect to the plane of the figure). Since the S-F bond pairs are alternatively stretched and compressed, the cluster structure preserving its axial symmetry, the monomer vibrations are enhanced by the overall cluster vibration and the resulting frequency shift is red, as can be seen from the stick spectrum in Fig. 15. In the case of the perpendicular vibration ($\perp$), from the symmetry of the components it follows that the fluorine atom cage indeed vibrates perpendicularly to the dimer axis, out of phase with respect to the sulphur atoms. The vibration is obviously doubly degenerate, rendering the cluster structure unsymmetrical. As a consequence, the valence S-F bonds are stretched on the whole, hindering the vibration of the implied fluorine atoms, and thus leading to a blueshift of the frequency.

The three pairs of van der Waals S-F bonds within the trimer are very similar to the ones in the second lowest

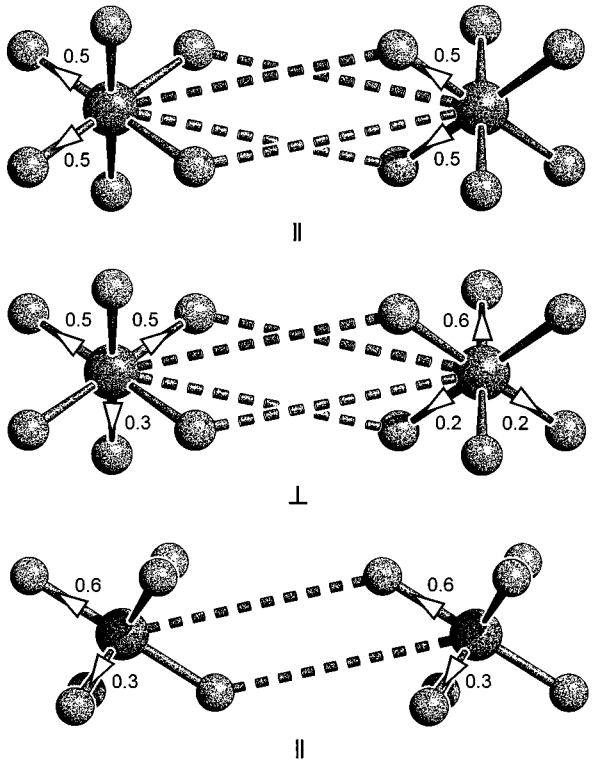

FIG. 16. The parallel and perpendicular vibrations (at 933.7 and 956.4 cm^{-1}) of the energetically lowest dimer isomer, and the parallel vibration (at 934.0 cm^{-1}) of the second lowest isomer.

dimer. Consequently, the parallel band of the trimer is expected to behave analogously with the parallel band of the second dimer and this is of course what is found in the stick spectrum of Fig. 15. Whereas, judging from the cyclic symmetry of the vibration components (Fig. 17), the $\perp_2$ band clearly corresponds to a perpendicular overall vibration with respect to the plane of the figure (with the fluorine and sulphur atoms moving out of phase up and down), the $\perp_1$ vibration also shows admixtures of in-plane vibrations, therefore being less blueshifted. In the case of the $\perp_2$ vibration, the out of phase movement of the fluorine atom cage and of the sulphur atoms results, as in the dimer case, in the van der Waals S-F bonds being stretched on the whole, which brings about the stiffening of the implied valence S-F bonds, and, thus, the blueshift of the vibration frequency.

In the case of the tetramer a qualitative new type of correlation occurs. The most stable tetramer (Fig. 18), seems to be built up from two transversely sandwiched second lowest dimers, within a slightly distorted T_d structure. A further finding, which results from the cyclic symmetry of the vibration vectors, is that the monomers constituting each ''dimer'' are strongly correlated, and therefore, the tetramer spectrum is expected to show roughly the structure encountered for the second lowest dimer. In the case of the $\|_2$ band at 935.9 cm^{-1}, the monomers vibrate pairwise in phase, the overall cluster vibration relaxing the bonds, and thus leading to a red frequency shift. On the contrary, in the case of the $\perp_2$ band at 965.1 cm^{-1} (practically overlapping the $\perp_1$ band), the monomers belonging to a certain ''dimer'' can be seen to vibrate

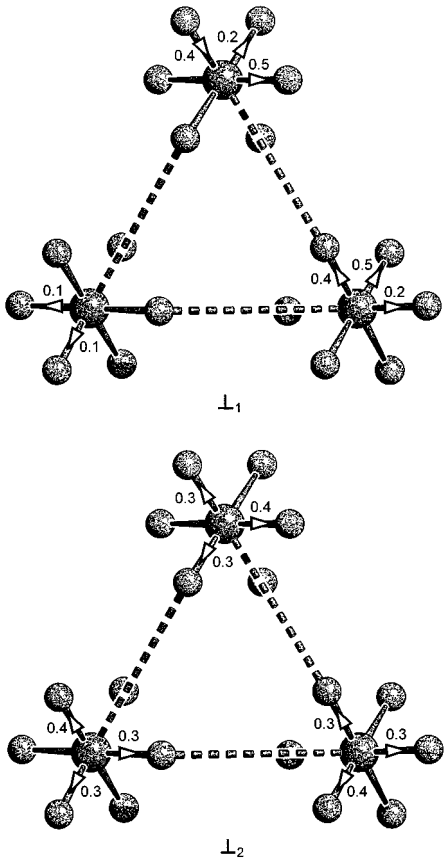

FIG. 17. The two perpendicular vibrations (at 958.9 and 964.4 cm^{-1}) of the most stable trimer.

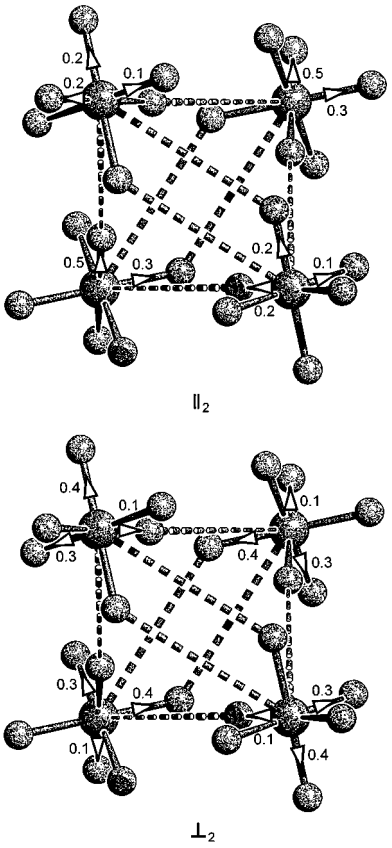

FIG. 18. The $\parallel_2$ and $\perp_2$ vibrations (at 935.9 and 965.1 cm^{-1}) of the most stable tetramer.

out phase. The S-S distances in the two composing ''dimers'' (on the diagonals of the depicted projection) alternatively increase and decrease in a hindered ''breathing'' motion. As a consequence, the individual monomer vibrations are hindered and a blue frequency shift results.

As for the second lowest tetramer (Fig. 19), the $\parallel_2$ band at 936.2 cm^{-1}, which is the first one to sensitively deviate from the so far hardly changed position of the parallel bands, is characterized by the vibration of the top monomer along the C_3 axis pointing to the onlooker, in phase with the symmetrical, predominantly in-plane torsion of the bottom ring. The character of parallel band clearly refers in this case to the collective vibration along the C_3 axis. The situation is reversed in the case of the $\perp_1$ band at 964.1 cm^{-1}, where the top monomer and the ring vibrate out of phase. Again the in phase vibrations are associated with redshifts, while the out of phase vibrations result in blueshifts.

IV. CONCLUSIONS

A new degenerate second order perturbation approach for evaluating the splitting and shifting of the vibrational bands of homogeneous molecular clusters is presented. The Hamiltonian of the system comprises harmonic and anharmonic intramolecular vibration terms, described in the normal mode representation, as well as the intermolecular potential. The degenerate monomer vibrational modes are being consistently taken into account. The anharmonic contributions of the intramolecular force field and the intermolecular potential are treated as a perturbation. The first order of the new perturbation approach appears to be a straightforward generalization of previous results from the literature.[11–13] In the second order, however, substantial formulation differences result from the consideration of the complete basis set of the state space, which allows for a full description of the couplings of the intramolecular vibrations through the intermolecular potential.

A new site-site intermolecular potential for SF_6, comprising exchange, dispersion, electrostatic, and induction contributions, is presented. The effective charges assigned to the atoms are chosen such as to account for the observed vibrational transition dipole moment of the SF_6 monomer. The dispersion coefficients for the individual atomic species are determined by fitting the calculated temperature dependence of the second virial coefficient of SF_6 to the experimental evidence. Two variants of our potential model (one neglecting the induction interactions, and the other one including them) are applied to compute SF_6 cluster structures up to the hexamer, which are compared with those obtained by using other potential models from the literature. The average S-S distance and the incremental cluster binding energy are employed to correlate the ''compactness'' of the found cluster structures with their symmetry properties. It is confirmed that SF_6 forms true van der Waals clusters, mainly bound by the dispersion attraction, the effect of the induction interactions being negligible.

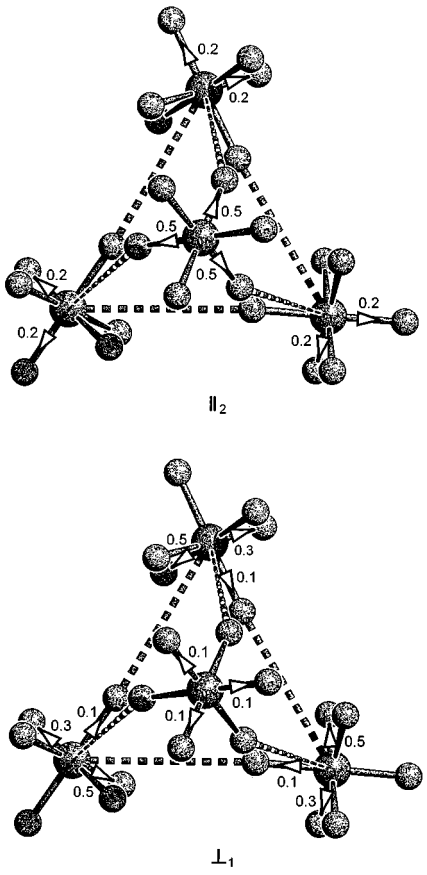

FIG. 19. The $\|_2$ and $\perp_1$ vibrations (at 936.2 and 964.1 cm^{-1}) of the second lowest tetramer.

The new second order line shift formalism is used to calculate the IR-spectra of the found SF_6 clusters in the region of the ν_3 vibrational mode. It is noted that, although much smaller than the first order frequency shifts, the second order ones are meaningful, achieving a fine-tuning of the calculated spectra. The contributions to the line shifts from the various interaction terms are analyzed and it is found that the electrostatic coupling is by far dominant. By a simple molecular multipole analysis, this large contribution can be attributed to the vibrational dipole-dipole interaction, which has been held responsible for the vibrational splittings in the literature. The calculated spectra compare favorably with data for clusters up to the tetramer (from IR-IR double resonance experiments and IR photo-dissociation experiments with size-selected clusters) and the overall better agreement of the results obtained neglecting induction over those including it, is apparent. The systematic redshift of the spectra for all cluster sizes renders the inclusion of the induction interaction with the available atomic polarizabilities inappropriate.

The structure of the cluster vibrations is investigated in terms of the individual monomer vibrations and is correlated with the found geometrical cluster configurations. The parallel bands are associated with in phase vibrations and result in red frequency shifts, due to the enhancement of the individual monomer vibrations by the overall cluster vibration, while the perpendicular bands imply out of phase vibrations producing blue frequency shifts, due to the hindering of the normal modes of the monomers.

ACKNOWLEDGMENTS

One of the authors (T.A.B) would like to express his thanks to Dr. K. Sunouchi for his continuous support in various aspects regarding the efficient usage of the computational environment. Thanks are also due to Dr. J. Onoe and to Dr. V. Tosa, for stimulating discussions and suggestions, and for providing explanations on experimental techniques.

APPENDIX A: EXPRESSIONS OF PERTURBATION MATRIX ELEMENTS

Making the notation

$$F_{rm}=\frac{\partial U}{\partial q_{rm}}+\frac{hc}{4}\sum_t \phi_{ttr},$$

we have the following non-vanishing perturbation matrix elements to be used in the derivation of the first order line shifts:

$$\langle 0|W|0\rangle = U_0+\frac{1}{4}\sum_r \sum_m \frac{\partial^2 U}{\partial q_{rm}^2},$$

$$\langle 1_{rm}|W|0\rangle = (1/\sqrt{2})F_{rm},$$

$$\langle 2_{rm}|W|0\rangle = \frac{1}{2\sqrt{2}}\frac{\partial^2 U}{\partial q_{rm}^2},$$

$$\langle 1_{rm}1_{sl}|W|0\rangle = \frac{1}{2}\frac{\partial^2 U}{\partial q_{rm}\partial q_{sl}},$$

$$\langle 3_{rm}|W|0\rangle = (hc/4\sqrt{3})\phi_{rrr},$$

$$\langle 2_{rm}1_{sm}|W|0\rangle = (hc/4)\phi_{rrs},$$

$$\langle 1_{rm}1_{sm}1_{tm}|W|0\rangle = (hc/2\sqrt{2})\phi_{rst}.$$

The non-vanishing perturbation matrix elements used for the derivation of the second order line shifts are the following:

$$\langle 0|W|1_{ni}\rangle = (1/\sqrt{2})F_{ni},$$

$$\langle 1_{rm}|W|1_{ni}\rangle = \left(U_0+\frac{1}{4}\sum_{r'}\sum_{m'}\frac{\partial^2 U}{\partial q_{r'm'}^2}\right)\delta_{rn}\delta_{mi} + \frac{1}{2}\frac{\partial^2 U}{\partial q_{rm}\partial q_{ni}},$$

$$\langle 2_{rm}|W|1_{ni}\rangle = [F_{rm}\delta_{rn}+(hc/4)\phi_{rrn}]\delta_{mi},$$

$$\langle 1_{rm}1_{sl}|W|1_{ni}\rangle = (1/\sqrt{2})[F_{rm}+(3hc/4)\phi_{ssr} \times(1-\delta_{rs})\delta_{ml}]\delta_{sn}\delta_{li}+(1/\sqrt{2})[F_{sl} +(3hc/4)\phi_{rrs}(1-\delta_{rs})\delta_{ml}]\delta_{rn}\delta_{mi} +(hc/2\sqrt{2})\phi_{nrs}(1-\delta_{rs})(1-\delta_{rn}) \times(1-\delta_{sn})\delta_{mi}\delta_{li},$$

$$\langle 3_{rm}|W|1_{ni}\rangle=\frac{1}{2}\sqrt{\frac{3}{2}}\frac{\partial^2 U}{\partial q_{rm}^2}\,\delta_{rn}\delta_{mi},$$

$$\langle 2_{rm}1_{sl}|W|1_{ni}\rangle=\frac{1}{2\sqrt{2}}\frac{\partial^2 U}{\partial q_{rm}^2}\,\delta_{sn}\delta_{li}+\frac{1}{\sqrt{2}}\frac{\partial^2 U}{\partial q_{rm}\partial q_{sl}}\,\delta_{rn}\delta_{mi},$$

$$\langle 1_{rm}1_{sl}1_{tk}|W|1_{ni}\rangle=\frac{1}{2}\left(\frac{\partial^2 U}{\partial q_{rm}\partial q_{sl}}\,\delta_{tn}\delta_{ki}+\frac{\partial^2 U}{\partial q_{sl}\partial q_{tk}}\,\delta_{rn}\delta_{mi}+\frac{\partial^2 U}{\partial q_{tk}\partial q_{rm}}\,\delta_{sn}\delta_{li}\right),$$

$$\langle 4_{rm}|W|1_{ni}\rangle=(hc/2\sqrt{3})\,\phi_{rrr}\delta_{rn}\delta_{mi},$$

$$\langle 3_{rm}1_{sl}|W|1_{ni}\rangle=(hc/4\sqrt{3})[\,\phi_{rrr}\delta_{sn}\delta_{li}+3\,\phi_{rrs}\times(1-\delta_{rs})\,\delta_{rn}\delta_{mi}],$$

$$\langle 2_{rm}2_{sl}|W|1_{ni}\rangle=(hc/2\sqrt{2})(\,\phi_{rrs}\delta_{sn}+\phi_{ssr}\delta_{rn})\times(1-\delta_{rs})\,\delta_{mi}\delta_{li},$$

$$\langle 2_{rm}1_{sl}1_{tk}|W|1_{ni}\rangle=(hc/4)[\,\phi_{rrs}(1-\delta_{rs})\,\delta_{ml}\delta_{tn}\delta_{ki}+\phi_{rrt}(1-\delta_{rt})\,\delta_{mk}\delta_{sn}\delta_{li}]+(hc/2)\,\phi_{rst}(1-\delta_{rs})(1-\delta_{rt})\times(1-\delta_{st})\,\delta_{rn}\delta_{mi}\delta_{li}\delta_{ki},$$

$$\langle 1_{rm}1_{sl}1_{tk}1_{uj}|W|1_{ni}\rangle=(hc/2\sqrt{2})[\,\phi_{rst}(1-\delta_{rs})(1-\delta_{st})(1-\delta_{tr})\,\delta_{ml}\delta_{mk}\delta_{un}\delta_{ji}+\phi_{stu}(1-\delta_{st})(1-\delta_{tu})(1-\delta_{us})\,\delta_{lk}\delta_{kj}\delta_{rn}\delta_{mi}+\phi_{tur}(1-\delta_{tu})(1-\delta_{ur})(1-\delta_{rt})\,\delta_{kj}\delta_{jm}\delta_{sn}\delta_{li}+\phi_{urs}(1-\delta_{ur})(1-\delta_{rs})(1-\delta_{su})\,\delta_{jm}\delta_{ml}\delta_{tn}\delta_{ki}].$$

APPENDIX B: POTENTIAL DERIVATIVES

The intermolecular potential derivatives with respect to a particular monomer vibrational coordinate, implied by the expressions of the frequency shifts, can be evaluated basically by displacing the atoms along the vibrational coordinate. With a view to this transformation it is useful to recall the linear relationship between the Cartesian displacement coordinates $d_{a\alpha}$ and the normal coordinates Q_r:

$$d_{a\alpha}=\sum_r\, m_a^{-1/2}l_{a\alpha}^r Q_r=\sum_r\,\tilde{l}_{a\alpha}^r q_r, \tag{B1}$$

used as part of the G-F method of Wilson.[15] Here m_a is the mass of atom a, $\alpha=(x,y,z)$ represents the Cartesian coordinate index, and $l_{a\alpha}^r$ are l-matrix elements, which can be interpreted as derivatives of the Cartesian displacement coordinates $d_{a\alpha}$ with respect to the normal coordinates Q_r. The dimensionless normal coordinates q_{rm} being given in terms of the standard normal coordinates Q_{rm} by $q_{rm}=\sqrt{2\pi c\omega_r/\hbar}\,Q_{rm}$, we obtain

$$\tilde{l}_{a\alpha}^r=\sqrt{\hbar/2\pi c\omega_r m_a}\,l_{a\alpha}^r. \tag{B2}$$

For a particular molecule m of the cluster, relation (B1) takes the form

$$d_{a\alpha}^m=\sum_r\,\sum_{\alpha'}\,A_{\alpha\alpha'}^m\tilde{l}_{a\alpha'}^r q_{rm}, \tag{B3}$$

with $A_{\alpha\alpha'}^m$ the rotation matrix which characterizes the position of the molecule within the cluster.

Considering the potential U as explicit function of the Cartesian coordinates of the individual atoms, its first order derivatives in the space of the normal coordinates may be approximated by the simple finite difference scheme:

$$\frac{\partial U}{\partial q_{rm}}=\frac{U(\ldots,\{x_{a\alpha}^m+\tilde{l}_{a\alpha}^{rm}h\},\ldots)-U_0}{h}+O(h^2),$$

where $\{x_{a\alpha}^m\}$ are the equilibrium Cartesian coordinates of the atoms in molecule m, while $\tilde{l}_{a\alpha}^{rm}h$ are the corresponding displacements for the h displacement of the normal coordinate q_{rm}. The arguments $x_{a\alpha}^m+\tilde{l}_{a\alpha}^{rm}h$ are in fact truncated power series of the Cartesian coordinates with respect to the normal coordinate increment. The second order derivatives may be obtained in principle by straightforward generalization. However, due to the instability of the above discretization scheme, we actually use in our calculations an $O(h^4)$ four-point formula. For the homogeneous second order derivatives we employ five-point relations of the same accuracy, while, for the mixed second order derivatives, $O(h^2)$ seven-point formulas are being used.[31] Nevertheless, the displacement of the atoms along the normal coordinates is performed according to the outlined principles. The optimum step size h was found to be 0.001 Å (one cannot take arbitrary low discretization step sizes, without being faced with severe round-off errors).

APPENDIX C: THE CLUSTER TRANSITION DIPOLE MOMENT

The Cartesian components of the transition dipole moment of the cluster can be defined as:

$$\mu_\alpha=\sum_m\,\sum_a\,q_a d_{a\alpha}^m,\quad \alpha=x,y,z,$$

where q_a is the charge associated with atom (site) a, and $d_{a\alpha}^m$ represents the Cartesian displacement of atom a from molecule m along direction α. Employing Eq. (B3), which

gives the relationship between Cartesian and normal coordinates through the l-matrix, the components of the cluster transition dipole moment for the transition from the initial state $|\Psi_0\rangle$ to the final state $|\Psi_n^i\rangle$ take the form:

$$\langle\Psi_n^i|\mu_\alpha|\Psi_0\rangle=\sum_r\sum_m\left[\sum_a q_a\sum_{\alpha'}A_{\alpha\alpha'}^m\tilde{l}_{a\alpha'}^r\right]\langle\Psi_n^i|q_{rm}|\Psi_0\rangle.$$

Considering in the above formula the 0th order approximations of the state vectors corresponding to fundamental excitations,

$$|\Psi_0\rangle\equiv|0\rangle,|\Psi_n^i\rangle\equiv|0\rangle_n^i=\sum_{n'\in\Gamma}\sum_{i'=1}^{M}c_{n'i',ni}|1_{n'i'}\rangle,$$

with coefficients $c_{n'i',ni}$ resulting from the eigenvalue problem (9), and replacing the implied matrix elements of the normal coordinate, $\langle 1_{n'i'}|q_{rm}|0\rangle=(1/\sqrt{2})\delta_{n'r}\delta_{i'm}$, we obtain:

$$\mu_{01}^\alpha\equiv{}_n^i\langle 0|\mu_\alpha|0\rangle$$
$$=\frac{1}{\sqrt{2}}\sum_{n'\in\Gamma}\sum_m\left[\sum_a q_a\sum_{\alpha'}A_{\alpha\alpha'}^m\tilde{l}_{a\alpha'}^{n'}\right]c_{n'm,ni}^*.$$

In the case of the monomer, the above expression simplifies to:

$$\mu_{01}^\alpha=\frac{1}{\sqrt{2}}\sum_a q_a\tilde{l}_{a\alpha}^n.$$

[1] J. Geraedts, S. Stolte, and J. Reuss, Z. Phys. A **304**, 167 (1982).
[2] J. Geraedts, M. Waayer, S. Stolte, and J. Reuss, Faraday Discuss. Chem. Soc. **73**, 375 (1982).
[3] M. Snels and R. Fantoni, Chem. Phys. **109**, 67 (1986).
[4] M. Snels and J. Reuss, Chem. Phys. Lett. **140**, 543 (1987).
[5] F. Huisken and M. Stemmler, Chem. Phys. **132**, 351 (1989).
[6] B. Heijmen, A. Bizzarri, S. Stolte, and J. Reuss, Chem. Phys. **132**, 331 (1989).
[7] J. W. I. van Bladel and A. van der Avoird, J. Chem. Phys. **92**, 2837 (1989).
[8] U. Buck and H. Meyer, Phys. Rev. Lett. **52**, 109 (1984).
[9] K. Fox and W. B. Person, J. Chem. Phys. **64**, 5218 (1976).
[10] K. Kim, R. S. McDowell, and W. T. King, J. Chem. Phys. **73**, 36 (1980).
[11] T. A. Beu, Z. Phys. D **31**, 95 (1994).
[12] A. D. Buckingham, Proc. R. Soc. London Ser. A **248**, 169 (1958); **255**, 32 (1960); Trans. Faraday Soc. **56**, 753 (1960).
[13] U. Buck and B. Schmidt, J. Chem. Phys. **98**, 9410 (1993).
[14] A. Dalgarno, in *Quantum Theory*, edited by D. R. Bates (Academic, New York, 1961).
[15] E. B. Wilson, J. C. Decius, and P. C. Cross, *Molecular Vibrations* (McGraw-Hill, New York, 1955).
[16] G. Herzberg, *Molecular Spectra and Molecular Structure. II. Infrared and Raman Spectra of Polyatomic Molecules* (Van Nostrand, Toronto, 1945), p. 123.
[17] C. W. F. T. Pistorius, J. Chem. Phys. **29**, 1328 (1958).
[18] V. C. Ewing and L. E. Sutton, Trans. Faraday Soc. **59**, 1241 (1963).
[19] R. S. McDowell, J. P. Aldridge, and R. F. Holland, J. Phys. Chem. **80**, 1203 (1976).
[20] L. Hedberg and I. M. Mills, J. Mol. Spectrosc. **160**, 117 (1993).
[21] A. R. Hoy, I. M. Mills, and G. Strey, Mol. Phys. **24**, 1265 (1972).
[22] M. A. Spackman, J. Chem. Phys. **85**, 6579 (1986).
[23] R. G. Gordon and Y. S. Kim, J. Chem. Phys. **56**, 3122 (1972).
[24] J. O. Hirschfelder, C. F. Curtiss, and R. B. Bird, *Molecular Theory of Gases and Liquids* (Wiley, New York, 1954).
[25] A. H. Stroud, *Approximate Calculation of Multiple Integrals* (Prentice-Hall, Englewood Cliffs, NJ, 1971).
[26] D. J. Evans and R. O. Watts, Mol. Phys. **28**, 1233 (1974).
[27] J. H. Dymond and E. B. Smith, *The Virial Coefficient of Gases* (Clarendon, New York, 1969).
[28] B. M. Powell, M. T. Dove, G. S. Pawley, and L. S. Bartell, Mol. Phys. **62**, 1127 (1987).
[29] A. Boutin, J.-B. Maillet, and A. H. Fuchs, J. Chem. Phys. **99**, 9944 (1993).
[30] A. Boutin, B. Rousseau, and A. H. Fuchs, Chem. Phys. Lett. **218**, 122 (1994).
[31] P. J. Davis and I. Polonsky, in *Handbook of Mathematical Functions*, edited by M. Abramowitz and I. A. Stegun (Dover, New York, 1972), pp. 883–884.